

## Controlling high-latitude Southern Ocean convection in climate models



Achim Stössel <sup>a,\*</sup>, Dirk Notz <sup>b</sup>, F. Alexander Haumann <sup>c</sup>, Helmuth Haak <sup>b</sup>, Johann Jungclaus <sup>b</sup>, Uwe Mikolajewicz <sup>b</sup>

<sup>a</sup> Department of Oceanography, Texas A&M University, College Station, USA

<sup>b</sup> Max-Planck-Institut für Meteorologie, Hamburg, Germany

<sup>c</sup> Environmental Physics, Institute of Biogeochemistry and Pollutant Dynamics & Center for Climate Systems Modeling, ETH Zürich, Switzerland

### ARTICLE INFO

#### Article history:

Received 8 May 2014

Received in revised form 10 November 2014

Accepted 24 November 2014

Available online 18 December 2014

#### Keywords:

High-latitude Southern Ocean

Climate models

Surface buoyancy fluxes

Convection

Sea ice

### ABSTRACT

Earth System Models (ESMs) generally suffer from a poor simulation of the High-Latitude Southern Ocean (HLSO). Here we aim at a better understanding of the shortcomings by investigating the sensitivity of the HLSO to the external freshwater flux and the horizontal resolution in forced and coupled simulations with the Max-Planck-Institute Ocean Model (MPIOM). Forced experiments reveal an immediate reduction of open-ocean convection with additional freshwater input. The latter leads to a remarkably realistic simulation of the distinct water-mass structure in the central Weddell Sea featuring a temperature maximum of +0.5 °C at 250 m depth. Similar, but more modest improvements occur over a time span of 40 years after switching from a forced to a coupled simulation with an eddy-resolving version of MPIOM. The switch is accompanied with pronounced changes of the external freshwater flux and the wind field, as well as a more realistic heat flux due to coupling. Similar to the forced freshwater-flux experiments, a heat reservoir develops at depth, which in turn decreases the vertically integrated density of the HLSO and reduces the Antarctic Circumpolar Current to rather realistic values. Coupling with a higher resolution version of the atmosphere model (ECHAM6) yields distinct improvements of the HLSO water-mass structure and sea-ice cover. While the coupled simulations reveal a realistic amount of Antarctic runoff, its distribution appears too concentrated along the coast. Spreading the runoff over a wider region, as suggested in earlier studies to mimic the effect of freshwater transport through icebergs, also leads to noticeable improvements of the HLSO water-mass properties, predominantly along the coast. This suggests that the spread of the runoff improves the representation of Antarctic Bottom Water formation through enhanced near-boundary convection rather than weakened open-ocean convection.

© 2014 Elsevier Ltd. All rights reserved.

### 1. Introduction

Earth System Models (ESMs) suffer from a poor representation of the High-Latitude Southern Ocean (HLSO) (e.g., Russell et al., 2006; Sloyan and Kamenkovich, 2007; Weijer et al., 2012; Sallée et al., 2013; Heuzé et al., 2013). This was the case for the climate-model simulations carried out for the fourth assessment report of the IPCC (e.g., Lemke et al., 2007; Meehl et al., 2007), and also applies to the simulations of the fifth coupled model inter-comparison project (CMIP5) that form the basis for the fifth assessment report IPCC-AR5. The shortcomings manifest themselves e.g. in the fact that CMIP5 ESMs usually simulate excessive interannual variability of the Southern Ocean (SO) sea-ice cover (e.g., Zunz et al., 2013; Turner et al., 2013). This is coupled to the representation of winds and the hydrographic properties of the HLSO, which

in turn depend on the surface buoyancy fluxes, and thus on the representation of sea ice. In this contribution, we explore the sensitivity of the HLSO in ESMs to ultimately determine the main controlling factors for an improved representation of the water-mass properties, of sea ice, and of the strength of the Antarctic Circumpolar Current (ACC). With HLSO we refer to the region south of the ACC, i.e. generally the region south of 60°S.

Much attention has been given to the question why most ESMs simulate a decreasing SO sea-ice cover in recent decades whereas satellite-derived sea ice shows a slight increase (e.g., Maksym et al., 2012; Parkinson and Cavalieri, 2012). Based on satellite-derived sea-ice drift and atmospheric reanalysis winds, Holland and Kwok (2012) explain the net upward trend in total SO sea-ice area by regional changes in the wind fields. The failure of ESMs to reproduce this upward trend is therefore at least in part linked to their failure to reproduce the observed regional trends in winds (e.g., Haumann et al., 2014). The model representation of regional winds in general is particularly relevant in Antarctic coastal

\* Corresponding author.

regions, where the wind fields are strongly affected by orography (e.g., Mathiot et al., 2010; Stössel et al., 2011; Vihma et al., 2011). The coastal wind fields influence the formation of coastal polynyas and thus the formation rate of Antarctic Bottom Water (AABW) through near-boundary convection (e.g., Carmack, 1990). Changes in the volume of AABW affect its northward extension along the deep western boundaries. In the Atlantic it modulates the outflow of North Atlantic Deep Water (NADW) (e.g., Hall et al., 1997; Hogg and Zenk, 1997; Stössel and Kim, 2001; Stössel et al., 2002; Cheon and Stössel, 2009), which in turn influences the long-term properties of Circumpolar Deep Water (CDW) and thus the stratification of the HLSO (e.g., Park and Latif, 2008; Martin et al., 2013; Cheon et al., 2014).

Enhanced atmospheric CO<sub>2</sub> causes a poleward shift of the westerlies (e.g., Oke and England, 2004; Toggweiler et al., 2006; Fyfe et al., 2007) thus causing a stronger negative wind stress curl over the HLSO. The latter implies a strengthening of the Weddell Sea (WS) and Ross Sea (RS) gyres, a more pronounced doming of isopycnals, and thus a more likely preconditioning for open-ocean convection (e.g., Gordon and Huber, 1990; Cheon et al., 2014). On the other hand, open-ocean convection will decrease in a warmer climate because of changes in the hydrological cycle (de Lavergne et al., 2014; Gordon, 2014). Most directly, warming leads to more precipitation over the SO (e.g., Knutti and Sedláček, 2013). This strengthens the ocean stratification, thus reducing upward ocean heat flux in the HLSO, which in turn will temporarily increase the concentration and/or thickness of sea ice (e.g., Bitz et al., 2005; Zhang, 2007; Gordon et al., 2007; Massonnet et al., 2013). In addition, more snow on sea ice will increase the amount of snow–ice formation, which contributes to sea-ice thickening (e.g., Powell et al., 2005; Maksym and Markus, 2008). Furthermore, while atmospheric warming leads to an overall reduction in ice growth, the associated reduction in oceanic heat flux may reduce ice melt to the point that the overall ice cover turns thicker and more compact in regions of initially strong convection (Zhang, 2007). Kirkman and Bitz (2011) argue that this effect is much stronger than the expected change in precipitation. Another major surface freshwater input in the HLSO is glacial melt water (e.g., Bintanja et al., 2013) though its significance for explaining the recent SO sea-ice increase has been disputed by Swart and Fyfe (2013).

Another line of reasoning to explain the increased sea-ice cover in the Southern Ocean relates to internal variability and internally driven long-term trends (e.g., Goosse et al., 2009; Martin et al., 2013). In two multiple-1000-year simulations with the coupled Kiel Climate Model (ECHAM5-NEMO-LIM), Martin et al. (2013) find the mode of open-ocean convection in the WS changing from a stage of deep convection to a stage of no convection and back on time scales of 50 to several 100 years. They explain this by the buildup of a heat reservoir during a no convection phase up to the point when the water column becomes unstable. The transition back to a mode of no convection is explained through gradual surface freshening, the eventual switch being triggered by seasonal sea-ice melt passing a certain threshold value. This study suggests that the trend in sea ice over the last 40 years could simply be due to multi-decadal changes in open-ocean convection. The CMIP5 analysis of de Lavergne et al. (2014), on the other hand, suggests that models that are convecting during the preindustrial era all switch to a non-convection mode in the future with no point of return (Gordon, 2014).

Most ESMs reveal significant biases in HLSO water-mass characteristics (e.g., Orsi and Whitworth, 2005; Russell et al., 2006; Close and Goosse, 2013; Sallée et al., 2013). This issue is to first order linked to the question of how AABW is being formed in individual models, i.e. either predominantly by open-ocean convection, or by near-boundary convection (e.g., Carmack, 1990; Marshall and

Schott, 1999; Heuzé et al., 2013). According to current understanding and to what has been observed over the past decades, it seems that near-boundary convection including the process of entrainment during downslope flow is the dominant mechanism determining the formation rate and properties of AABW. From that point of view, nature may already have shifted to a permanent mode of no open-ocean convection due to anthropogenic CO<sub>2</sub> emission. Furthermore, models showing excessive convection may not be wrong but rather reflect conditions of the recent past due to different boundary conditions such as a negative Southern Annular Mode (SAM) index (e.g., Thompson and Solomon, 2002; Gordon et al., 2007; Cheon et al., 2014).

To better understand the sensitivity of the various interacting processes controlling the distinct HLSO hydrography, we here analyze a set of uncoupled and coupled simulations with different versions of the current state-of-the-science ocean and climate model developed at the Max-Planck-Institute for Meteorology (MPI). This model, as many other CMIP5 models, features excessive open-ocean convection in the HLSO in its standard setup (e.g., Jungclaus et al., 2013; Close and Goosse, 2013; Sallée et al., 2013; de Lavergne et al., 2014) compared to HLSO conditions observed over the last 30 years. This deficiency has already been noticed in Griffies et al. (2009), who compared the performance of various sea-ice – ocean GCMs, all using presumably identical forcing fields. A critical variable affecting open-ocean convection in the HLSO is the external freshwater flux, e.g. in form of glacial melt water (e.g., Marsland and Wolff, 2001). We therefore start with investigating this effect in a set of uncoupled simulations. We then analyze the changes that occurred in an existing elaborate eddy-resolving version of the MPI ocean model when switching from uncoupled to coupled simulations, focusing on the short-term adjustment of the HLSO water masses over a time span of ~50 years after coupling. Toward the end, this is being compared to long-term results after several 1000 years of coupled integration that contributed to CMIP5, and the outcome of a sensitivity study on the impact of redistributing glacial meltwater in a coupled simulation. Our strategy is to approach the problem using different model variants (model resolution, initial conditions, forced versus coupled) to eventually determine how to properly balance the dominant processes controlling the HLSO of coupled ESMs.

In the following Section 2, we describe our analysis strategy and experimental designs. In Section 3, we show results from two sets of numerical experiments, focusing on the spatial distribution of integrated variables such as water-column mean density, mean external freshwater flux, sea-ice thickness and surface heat fluxes. The interaction between these variables and the resulting quality of HLSO water properties is discussed in Section 4. In Section 5, we summarize the main findings and conclude by investigating the effect of redistributed glacial meltwater in an additional experiment.

## 2. Analysis strategy and model setup

For our analysis, we use different model setups all including the MPI Ocean Model MPIOM. This model has been used in numerous studies (e.g., Jungclaus et al., 2006; Müller et al., 2010) and forms the sea-ice – ocean component of the MPI-ESM that contributed, for example, to the IPCC-AR5 projections (Jungclaus et al., 2013; Notz et al., 2013). We either use MPIOM in a stand-alone setup forced with atmospheric reanalysis/climatology, or coupled to ECHAM6, which constitutes the state-of-the-science atmosphere model component of MPI-ESM (e.g., Stevens et al., 2013).

We also use MPIOM and ECHAM6 at different resolutions. High-resolution simulations revealed substantial improvements in the representation of HLSO water masses and ACC strength (see

Section 3) upon switching from forced to coupled mode of operation. To understand this behavior, sensitivity experiments were conducted with the low-resolution ( $1.5^\circ$ ) version of MPIOM (MPIOM/GR15, in the following simply called GR15), which served as the ocean component of the low-resolution coupled model MPI-ESM-LR that was used for most CMIP5 experiments (Jungclaus et al., 2013). GR15 has a bipolar grid configuration with the poles over Greenland and Antarctica. Some of our sensitivity experiments were motivated by the study of Griffies et al. (2009), where GR15 was one of 4 models (of a total of 7) that delivered excessively deep mixed layers south of the ACC (their Fig. 15 top right) and a substantial over-estimation of the ACC strength (185 Sv; estimates derived from measurements amount to  $135 \pm 20$  Sv (e.g., Whitworth and Peterson, 1985; Cunningham et al., 2003)). In addition to the effect of salinity restoring (not shown), we investigated the impact of additional freshwater input, in particular following the hypothesis that the external freshwater supply provides a dominant control over convection and thus the overall water-mass properties of the HSO. The reference simulation without additional freshwater flux is termed “REF”. Besides precipitation, the freshwater input into the HSO is to a large extent determined by runoff from the Antarctic continent in form of glacial meltwater and icebergs (e.g., Gladstone et al., 2001; Beckmann and Goosse, 2003; Silva et al., 2006; Martin and Adcroft, 2010; Jongma et al., 2009; Tournadre et al., 2012; Bintanja et al., 2013; Weber et al., 2014). There are large uncertainties in the estimates of the rate and spread of glacial melt water from Antarctica. Gladstone et al. (2001) reported regional values south of  $65^\circ\text{S}$  of up to 0.5 m/year. Deriving iceberg trajectories by means of satellite remote sensing, Tournadre et al. (2012) estimate regional freshwater fluxes due to melting icebergs north of  $65^\circ\text{S}$  up to 0.3 m/year. To investigate the possible impact of an overall larger freshwater flux, we followed Marsland and Wolff (2001) by simply adding a fixed rate of freshwater input south of  $60^\circ\text{S}$ , estimating an upper bound of the possible response by using an unrealistically high value of 1 m/year (experiment “FW”).

The atmospheric forcing field used for the GR15 experiments are based on the OMIP climatology (Röske, 2006). These “GR15-OMIP” experiments start from rest with climatological ocean properties according to NODC\_WOA98 (<http://www.esrl.noaa.gov/psd/>) and were run for 50 years (Table 1). This is clearly not enough time for the global overturning circulation to adjust, but sufficient for our main aim to investigate the initial adjustment of the HSO density structure and the tendency of the strength of the ACC without the long-term impact of possible changes in the outflow of NADW that would ultimately affect the abundance and property of CDW. The two forced experiments are subject to salinity restoring where

there is no ice. The associated time constant can be converted into a “piston velocity” [m/s] which translates into a freshwater flux  $q = -v_p (S_{\text{obs}} - S_{\text{mod}})/S_{\text{mod}}$ , where  $v_p$  is the piston velocity,  $S_{\text{obs}}$  is the observed salinity, and  $S_{\text{mod}}$  is the modeled salinity (Griffies et al., 2009). Both forced GR15 experiments use  $v_p = 3.3 \cdot 10^{-7}$  m/s, which corresponds to a restoring time scale of 1.2 years over the upper-layer depth of 12.5 m.

The high-resolution experiments we examine are based on a tri-polar (TP) grid MPIOM version at  $0.1^\circ$  or 6 min (6M) horizontal resolution, MPIOM/TP6M (von Storch et al., 2012), in the following simply called TP6M. This high-resolution model setup features a substantially higher resolution of the bathymetry than GR15 and than the MPIOM version used in the CMIP5 intermediate-resolution setup MPI-ESM-MR (TP04, i.e. tripolar 0.4 degree horizontal resolution), in particular since all MPIOM versions feature partial grid cells (e.g., Maier-Reimer et al., 1993; Adcroft et al., 1997). This leads to a more detailed representation of the accumulation and overflow of dense shelf water (e.g., Orsi et al., 1999; Heuzé et al., 2013). The TP6M experiments we examine here constitute a sequence of simulations that started with 25 years of OMIP-climatology-forced MPIOM/TP6ML80 (from rest with NODC\_WOA98 ocean properties), where L80 stands for 80 vertical levels. This simulation continued for another 60 years with atmospheric forcing based on real-time 6-hourly NCEP reanalyses (von Storch et al., 2012). The end of that forced simulation was the starting point for 2 coupled simulations, namely MPIOM/TP6ML40-ECHAM6/T255 (in the following called TP6M-T255) and MPIOM/TP6ML40-ECHAM6/T63 (in the following called TP6M-T63), where T255 stands for spectral triangular truncation at wave number 255, and T63 correspondingly at wave number 63 (e.g., Washington and Parkinson, 2005).

Finally, the results of the forced GR15 and the coupled TP6M experiments are compared with those of the preindustrial control (piCon) simulations of MPI-ESM-LR (in MPI model name terminology MPIOM/GR15L40-ECHAM6/T63, and for our comparison simply GR15-T63-piCon). The piCon integrations were run for several thousand years in coupled mode with constant radiative forcing at preindustrial level. In these simulations, the global ocean overturning circulation and deep-ocean properties have equilibrated, and the HSO properties will include the long-term effect of changes in NADW outflow and properties.

Originating from GR15-T63-piCon, a coupled runoff experiment (GR15-T63-RO) was added to investigate the impact of spreading the Antarctic runoff (or glacial meltwater) over the entire ocean region south of  $60^\circ\text{S}$ . This is a crude representation of the spreading of melt water through icebergs. A more adequate implementation would be that of e.g. Martin and Adcroft (2010) where interactive

**Table 1**  
Annual-mean as well as south-of- $70^\circ\text{S}$  and south-of- $60^\circ\text{S}$  spatial-mean density below 200 m depth (referenced to surface pressure) [ $\text{kg}/\text{m}^3$ -1000] and external (excluding contributions from sea-ice growth or melt) freshwater (FW) flux [ $\text{cm}/\text{year}$ ], consisting of precipitation ( $P$ ), evaporation ( $E$ ), runoff, and FW flux from restoring when uncoupled, as well as ACC strength [ $\text{Sv}$ ] and wind-stress curl [ $\text{Pa}/\text{m} \cdot 10^{-7}$ ] over the ocean south of  $50^\circ\text{S}$  from all simulations considered and as derived from observations.

Experiments	Density <70S	FWF <70S	Density <60S	FWF <60S	$P - E$ <60S	Runoff <60S	Restoring <60S	ACC	Wind stress curl
GR15-OMIP-REF.50	27.85	34	27.84	47	26	9	12	195	-1.30
GR15-OMIP-FW.50	27.69	95	27.78	87	131 <sup>b</sup>	9	-53	142	-1.30
TP6M-NCEP.2010	27.88	57	27.87	73	44	9	20	230	-1.68
TP6M-T255.0	27.86	87	27.87	62	46	16	n/a	219	-1.27
TP6M-T255.40	27.70	79	27.81	59	47	12	n/a	141	-1.28
TP6M-T63.40	27.70	80	27.81	54	41	13	n/a	148	-1.52
TP6M-T63.90	27.70	80	27.81	56	43	13	n/a	135	-1.59
GR15-T63-piCon	27.64	61	27.71	47	37	11	n/a	160	-1.43
GR15-T63-RO.50	27.71	38	27.73	47	38	9	n/a	178	-1.49
Observations <sup>a</sup>	27.81	55	27.81	65	55	10	n/a	135	

<sup>a</sup> Some of the observed estimates bear large uncertainties (explanations and references see text).

<sup>b</sup> This figure includes specified additional freshwater flux (FW experiment).

icebergs are simulated as Lagrangian particles in an Eulerian framework.

For experiment identification we omitted “MPIOM” for forced experiments, and “MPIOM-ECHAM6” for coupled experiments, i.e. just indicated the MPIOM horizontal resolution and grid (e.g., GR15, TP6M), followed by the forcing (e.g., OMIP, NCEP) for the uncoupled experiments, and the resolution of ECHAM6 for the coupled experiments (e.g., T255, T63). Supplemental model experiments are flagged with REF (REFERENCE), FW (FreshWater), and RO (RunOff). Separated by a dot, this is augmented by the simulation year being investigated (e.g., year 40), or the actual year of real-time forcing (e.g., year 2010 of NCEP). All discussed experiments are listed in the left column of Table 1.

We mostly show results from the final simulation year of the sensitivity experiments. These are directly compared to the archived results of the TP6M experiments 40 to 90 years into coupled integration (i.e., as long as these expensive experiments have been run). Coupled simulations are generally prone to higher interannual variability than forced simulations, in particular for variables such as sea-ice concentration. Focusing on winter values we found that 5-year August means did not differ much from single-year August means, in particular not to the point that they would affect our main conclusions. For sea ice we nevertheless show 5-year August means, i.e. of the last 5 years of the respective sensitivity experiments or the respective stage of the TP6M experiments. The shown wind stress was treated similarly, but reflects 6-year means over entire years. Furthermore, the annual-mean ACC strength is shown as time series.

To analyze the quality of the simulations, we focus on a limited number of characteristic SO quantities. These include 2-d horizontal maps of vertical-mean density below 200 m, sea-ice thickness, external freshwater flux (defined as precipitation minus evaporation plus continental runoff of any sort, i.e. not including freshwater flux from thermodynamic sea-ice growth and melt), surface heat flux, and near-surface air temperature. 3-d fields that we examined include potential temperature, salinity, and potential density. An important indicator for model performance of the HLSO is the meridional water-mass distribution across the WS. A reliable source for its verification is WOCE repeat section A23 (e.g., Orsi and Whitworth, 2005). Since the meridional density gradient across the ACC is directly linked to its strength, this is also being monitored for each experiment. Other quantities are the meridional distribution of zonal wind stress and the wind-stress curl.

### 3. Results

Fig. 1 shows meridional sections of potential temperature, salinity and potential density along 30°W from the WOCE climatology, providing a typical picture of the HLSO water-mass properties, in this case through the WS gyre. The upper 50 to 100 m are characterized by temperatures close to the freezing point and relatively low salinity (note that measurements are generally summer biased). Deeper down is the core of the relatively warm (up to +0.5 °C) and saline (up to 34.69 g/kg) CDW at about 300 m depth extending all the way to the Antarctic continental margin where this core deepens to about 800 m. The density structure is mainly determined by the salinity distribution and the dynamics of the WS gyre, leading to a doming of isopycnals with a potential density maximum (referenced to 0 dbar) up to 1027.86 kg/m<sup>3</sup>.

The corresponding sections from August of TP6M-NCEP.2010 look distinctly different (Fig. 2). Irrespective of possible seasonal and interannual variability in the upper 200 m, the pattern shown in the figure is typical for forced MPIOM simulations (e.g., Griffies et al., 2009), illustrating the problem of excessive open-ocean convection. There are clearly major discrepancies to the measure-

ment-based climatology. While fronts across the ACC are readily discernable and constitute a realistic feature, the central WS gyre is completely mixed with no indication of CDW whatsoever. Furthermore, the temperature is at the surface freezing point throughout the water column. Salinity is vertically homogeneous at 34.7 g/kg. As a result of the excessively cold temperature throughout the water column, the density (>1029.0 kg/m<sup>3</sup>) is overestimated across much of the WS gyre. Note that the focus here is the water column below 200 m, i.e. below the part being affected by seasonality.

Table 1 lists all experiments discussed in this study together with a number of critical quantities. In TP6M-NCEP.2010 the strength of the ACC reaches up to 230 Sv. We note a remarkable improvement of the ACC strength upon coupling (TP6M-NCEP.2010 vs. TP6M-T255.40). A likely candidate for this improvement is the HLSO density that eventually determines the meridional density gradient across the ACC, and thus its strength (e.g. Pierce et al., 1995; Martin et al., 2013). To investigate this relationship, we calculated the 3d-spatially averaged August-mean density below 200 m south of 70°S and south of 60°S, respectively, which is given in Table 1 along with the annual-mean ACC strength. We neglect the upper 200 m so that changes in density are just due to changes in dense-water accumulation rather than due to the spreading of surface freshwater. For selected experiments, the ACC strength is also shown as time series over the respective integration periods (Fig. 3). Within the respective sets of experiments (separated by bold lines in Table 1) there is generally a close relationship between the HLSO density and the ACC strength, i.e. the denser the water south of the ACC, the stronger the ACC. Such relationship has also been noticed by Meijers et al. (2012) and Sallée et al. (2013), and is most pronounced for density south of 70°S. Observed estimates suggest a mean potential density value below 200 m south of 60°S of 1027.81 kg/m<sup>3</sup>, which compares favorably with the simulated HLSO density of the experiments with the lowest and most realistic strength of the ACC. On the other hand, the corresponding observed density south of 70°S being the same as that south of 60°S does not support it being strongly related to the ACC strength. In fact, this lack in meridional difference also holds for all forced experiments, suggesting that the less dense conditions south of 70°S in the coupled experiments have to do with the treatment of the Antarctic runoff (see discussion). The coupled GR15-T63 set of experiments shown in Table 1 will be discussed in Sections 4 and 5.

To investigate the distribution of density in more detail, we examine the horizontal distribution of vertical- and August-mean density below 200 m (Fig. 4). For a convenient comparison, the coarse-grid GR15 results and the fine-grid TP6M results have been interpolated onto a latitude-longitude grid that corresponds to the intermediate-resolution TP04 grid. GR15-OMIP-REF.50 yields high density in the central WS and RS gyres, as well as in the high-latitude embayments. This situation changes drastically when adding freshwater south of 60°S (GR15-OMIP-FW.50). This measure leads to a substantial reduction of density all along the Antarctic coastline, in particular including the high-latitude embayments. At the same time, this experiment features a reduction of the ACC from 195 Sv to 142 Sv within 50 years (Fig. 3).

Moving on to the eddy-resolving TP6M experiments, the density distribution of TP6M-NCEP.2010 resembles that of GR15-OMIP-REF.50, but the former yields overall noticeably denser water. Accordingly, the ACC strength of TP6M-NCEP.2010 is at 230 Sv even more overestimated than that of GR15-OMIP-REF.50 (Table 1). After 40 years of coupled integration the HLSO density has diminished substantially, in particular in the high-latitude embayments, similar to GR15-OMIP-FW.50. The density distribution of TP6M-T63.40 looks rather similar (not shown), as does the total density (Table 1). The ACC is consistently reduced to acceptable values (Table 1; Fig. 3). Except for the high-latitude

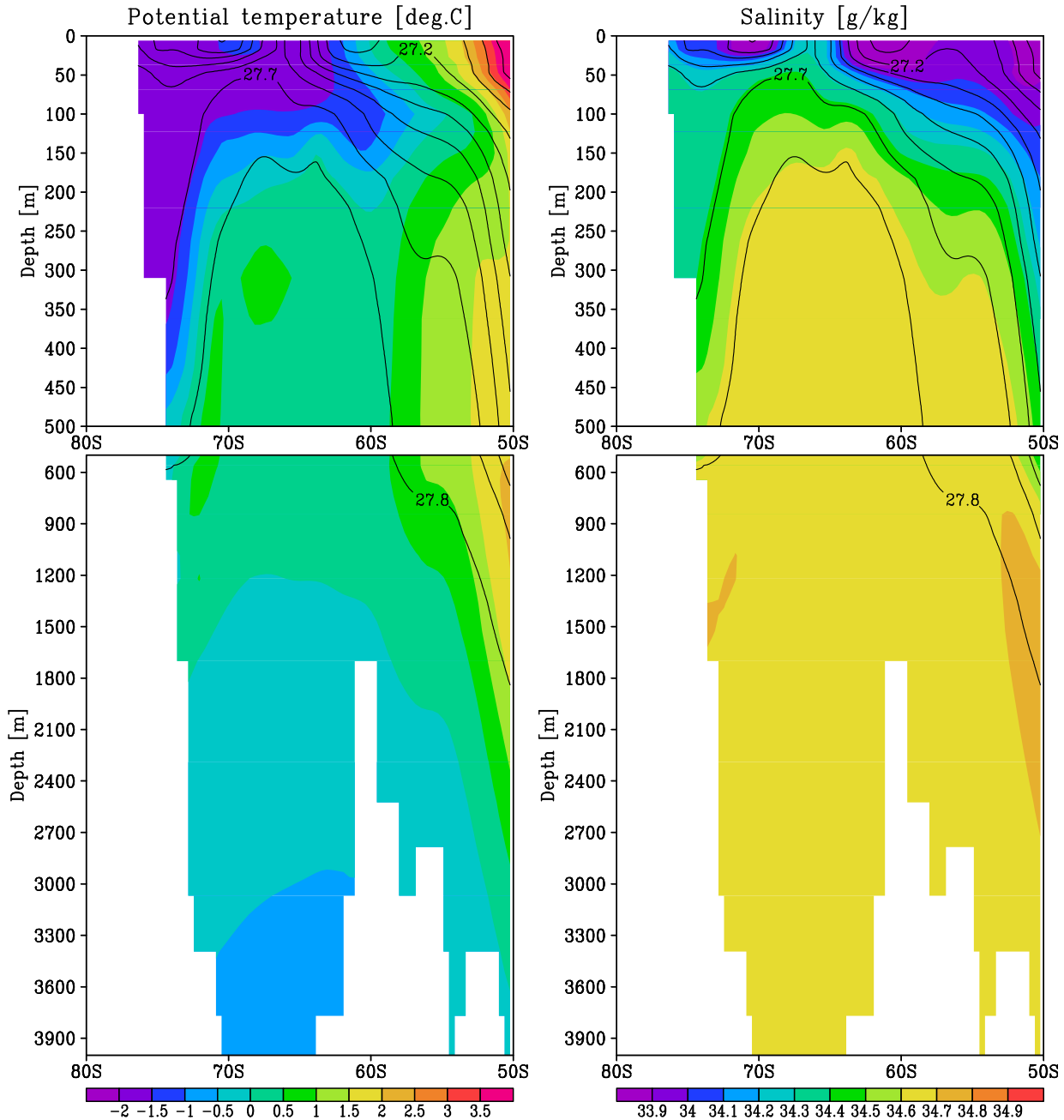


**Fig. 1.** Meridional sections along 30°W of potential temperature (left), salinity (right), and potential density (contours) from the WOCE climatology.

embayments, comparison with the WOCE data indicates that GR15-OMIP-FW.50 yields the most realistic result.

The multi-year August-mean sea-ice thickness is shown in Fig. 5. It provides a good indication of open-ocean convection and the underlying water-mass structure due to its direct response to the subsurface heat flux. In terms of sea-ice thickness, a measure of good performance is the relative thinness (about 0.5 m) of the majority of the wintertime ice pack (e.g., Worby et al., 2008; Zwally et al., 2008; Stössel, 2008). GR15-OMIP-FW.50 shows a clear increase of ice thickness versus GR15-OMIP-REF.50, which is due to enhanced stratification and reduced ocean heat flux. Upon coupling of TP6M, there is a similar tendency toward a thicker and more compact winter ice cover. On the other hand, there are regions in the eastern WS that are indicative of open-ocean polynyas in TP6M-T63.40 that do not emerge in TP6M-T255.40. Further-

more, the winter sea-ice cover of TP6M-T255 is more extensive than that of TP6M-T63. Noting that the coupling frequency in these two experiments is the same (hourly), these differences are only explicable through effects of the different spatial resolution of the atmosphere model. Except for the lacking RS polynya, GR15-OMIP-FW.50 yields the most realistic winter ice thickness, followed by TP6M-T255, which, however, suffers from an excessive extent in the Atlantic sector and too thick ice along East Antarctica.

To follow up on the hypothesis that the improvement of the ACC strength upon coupling is mainly due to changes in the HSO freshwater supply, Table 1 contains the spatially averaged annual-mean external freshwater flux broken down in precipitation minus evaporation and runoff (and implied freshwater flux from salinity restoring in the forced experiments), without considering contributions from sea-ice melt or growth. Except for TP6M-T255.0,

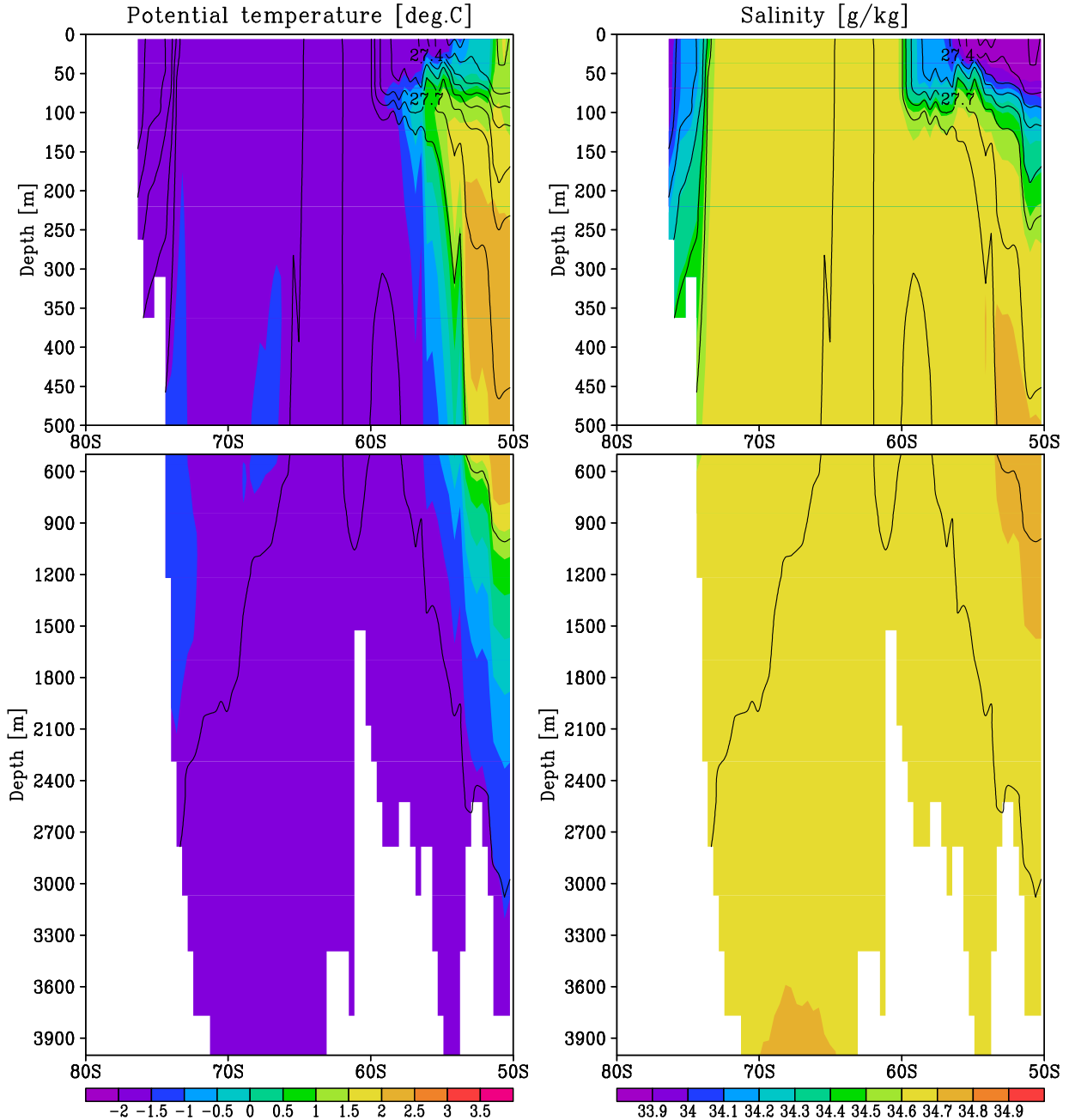


**Fig. 2.** Results from TP6M-NCEP.2010, August; otherwise as [Fig. 1](#).

which has not experienced any noticeable adjustment, there is a tendency for HLSO density below 200 m to decrease with an increase in external freshwater input mainly when both are restricted to south of 70°S, again suggesting that this may be an artifact of the treatment of the Antarctic runoff in the coupled models.

[Fig. 6](#) shows a considerable change in external freshwater flux between coupled and uncoupled experiments, and among the uncoupled experiments themselves (grey regions indicate negative freshwater flux). Switching from the uncoupled to the coupled TP6M simulations, the freshwater input into the SO generally diminishes except right along the Antarctic coastline and most of the WS, where the freshwater input actually increases (this is also reflected in [Table 1](#) for freshwater input south of 70°S). Even though the overall freshwater input south of 60°S decreased, the

HLSO turns less dense in the course of the 40 years of coupled integration, suggesting that a large amount of the freshwater south of 70°S is being advected northward where it potentially affects the stratification to the point that less dense water is being produced.

The forced simulations GR15-OMIP-REF.50 and TP6M-NCEP.2010 show extraction of freshwater (grey regions in [Fig. 6](#)), predominantly because of salinity relaxation. GR15-OMIP-FW.50 shows large positive values south of 60°S, as expected. Note that the salinity restoring acts against the freshwater anomaly in the amount of about 0.5 m/yr ([Table 1](#)). The coupled simulations, on the other hand, reveal a strong freshwater input along the coast of Antarctica. Initially, this leads to thinner ice, which recovers during the course of the coupled integration to thicker ice than in the forced simulation ([Fig. 5](#)), in particular in TP6M-T255. Further offshore, there is apparently more freshwater input into the SO in

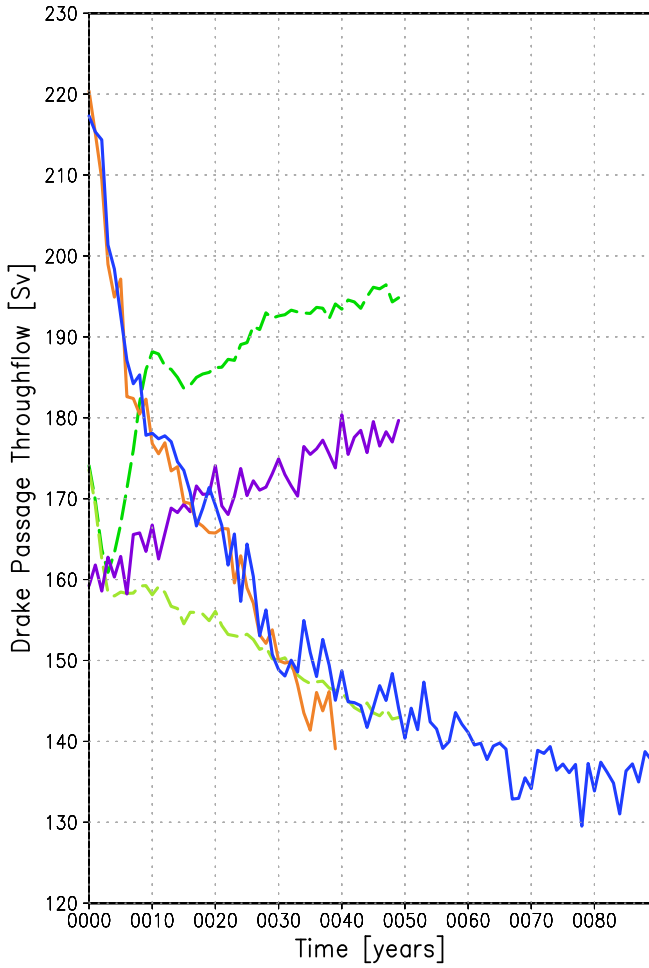


**Fig. 3.** Time series of annual-mean Drake Passage throughflow from uncoupled experiments GR15-OMIP experiments (colored dashed lines) REF (dark green) and FW (light green), and from coupled experiments (colored solid lines) TP6M-T255 (orange), TP6M-T63 (dark blue), and GR15-T63-RO (purple). (For interpretation of the references to colour in this figure legend, the reader is referred to the web version of this article.)

TP6M-NCEP.2010 than in the coupled TP6M simulations, except for the southern WS and RS. TP6M-T63 shows a coarser grid pattern because of the coarser AGCM resolution. Apparently the coarser grid leads to larger areas around Antarctica being exposed to enhanced freshwater flux than in TP6M-T255, though this is not reflected in the spatially averaged freshwater flux (Table 1).

The August-mean surface heat flux (not shown) is highly dependent on the ice cover, with the pattern of strong heat loss in the HLSO following that of low ice thickness and concentration. There is a considerable decrease of heat loss in GR15-OMIP-FW.50 versus GR15-OMIP-REF.50 as well as with a switch from uncoupled to coupled mode. The latter is to a large extent due to changes in the turbulent heat fluxes. These depend, besides wind speed, on the temperature and humidity differences between air and sea surface. In the coupled simulation, the air temperature and humidity are able to adjust to the surface conditions, which reduces the vertical gradient and hence the cooling due to turbulent heat fluxes. In the uncoupled case, the air temperature and humidity will remain at their specified values irrespective of the simulated surface conditions. This leads in winter to a situation of strong cooling in areas that are ice free or covered by thin ice. This difference can be seen in the August-mean 2-m air temperature (Fig. 7). The region of near-surface air temperature colder than  $-30^{\circ}\text{C}$  of the NCEP data

is obviously substantially larger than that of TP6M-T255.0, in particular in the RS, the WS, and along East Antarctica. The reduced cooling in the coupled simulations is a main contributor to reducing thermodynamic ice growth, and thus convection and dense-water formation. August-mean sea-surface salinity (Fig. 8) responds not only directly to the external freshwater flux, but also to brine and freshwater release due to freezing and melting. There is a distinct reduction of salinity in GR15-OMIP-FW.50. The reduction in surface salinity is even more pronounced in the sequence TP6M-NCEP.2010, TP6M-T255.40. While TP6M-T63 maintains equally low salinity near the coast of Antarctica, it yields higher salinity in the open ocean compared to TP6M-T255. The lower salinity along Antarctica in both TP6M-T255.40 and TP6M-T63.40 can be attributed to the larger runoff (Fig. 6), with salinity values similar to GR15-OMIP-FW.50.

Since standard forced MPIOM simulations are characterized by excessive open-ocean convection in the HLSO, it is revealing to investigate the temperature, salinity, and density profiles in the central WS (Fig. 9 top row), in the wider WS (Fig. 9 middle row), and in the circumpolar HLSO between  $60^{\circ}\text{S}$  and  $70^{\circ}\text{S}$  (Fig. 9 bottom row). These will first be analyzed for the TP6M simulations (colored solid lines except purple). Considering that the sequence of TP6M experiments started from an ocean climatology that reflects central WS profiles similar to the solid black lines in Fig. 9, it is remarkable that the temperature stratification in the WS disappears completely during the first 25 years of the OMIP-forced phase, at which point the temperature profile is totally homogeneous (not shown). Furthermore, the entire water column attains values close to the surface freezing point. After 60 years of 6-hourly real-time NCEP forcing a slight stratification develops, but with a maximum temperature of only  $-1.7^{\circ}\text{C}$  at 200 m depth (not shown). Immediately upon coupling (Fig. 9 top left, solid red line), a more pronounced wintertime maximum of  $-1.4^{\circ}\text{C}$  emerges at 250 m depth, which after 40 years of coupled simulation develops into a much more pronounced maximum of  $-0.2^{\circ}\text{C}$  at 300 m (solid orange line). By then the temperature profile has gained a shape much more similar to what is being observed, except that the maximum is still  $0.7^{\circ}\text{C}$  shy of the observed value. After 40 years of coupled simulation with the coarser AGCM (TP6M-T63.40), the shape of the temperature profile at that location is less realistic in that the maximum reaches only  $-0.8^{\circ}\text{C}$ , and is spread out from 400 m to 1500 m (solid dark blue line) rather than being more confined around a water depth of 300 m. After another 50 years of integration (TP6M-T63.90), the deeper layers are warming toward more realistic values (solid light blue line), which would presumably also happen in a corresponding continuation of TP6M-T255. However, there is no improvement of TP6M-T63.90 versus TP6M-T63.40 above 1700 m. The wider WS (Fig. 9 middle left) shows similar behavior, while in the circumpolar belt (Fig. 9 bottom left) TP6M-T63 shows a deterioration above 1800 m upon further integration. The inversion in the top 100 m of the WOCE profile stems from the fact that observed data is summer biased. The simulations also show a shallow stratification in summer (not shown).

As for salinity in the central WS (Fig. 9 top middle), the observed profile (solid black line) shows a summer bias in that its surface salinity is 0.2 g/kg lower than what would be expected in winter. This has been judged from the monthly Polar Hydrographic Climatology (PHC, Ermold and Steele, [psc.apl.washington.edu/Climatology.html](http://psc.apl.washington.edu/Climatology.html)) ocean data, which is available for that location up to a depth of 1400 m. Otherwise, the PHC profile is similar to the WOCE profile, in particular with respect to displaying a salinity maximum close to 34.69 g/kg at 300 m depth. Together with the temperature maximum at that depth, this is indicative of CDW. While the OMIP-forced spin-up run ends with a realistic salinity at depth (not shown), this high salinity value extends all

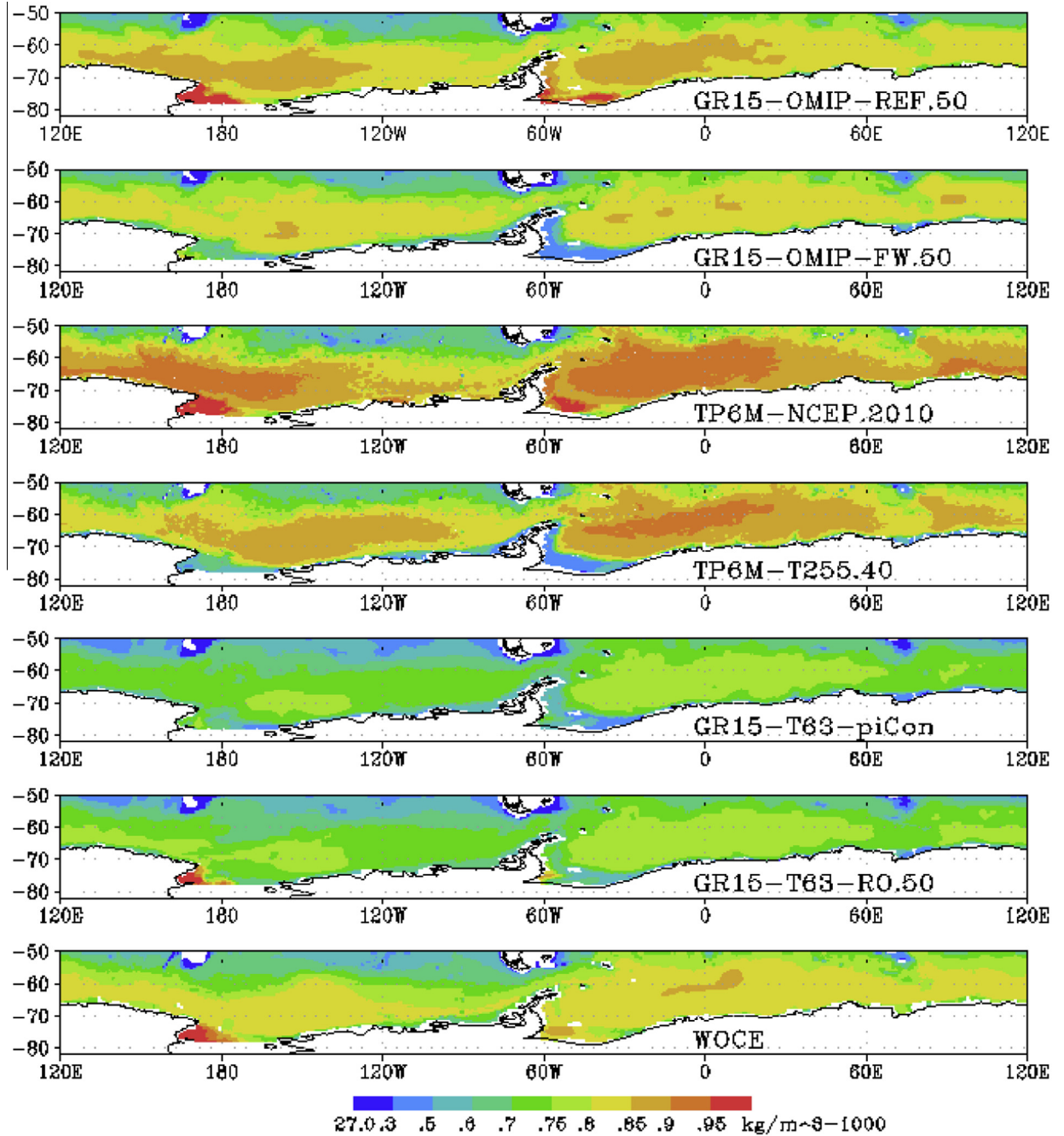


**Fig. 4.** August-mean, vertical-mean density below 200 m for indicated experiments and WOCE.

the way to the surface, again not showing any indication of stratification. During the 60 years of the NCEP-forced simulation, a weak salinity gradient builds up throughout the water column. By the end of that simulation, the salinity at depth has reached a value that is overestimated by 0.05 g/kg. One year into the coupled simulation (TP6M-T255.0), a weak halocline emerges (solid red line) that develops into a pronounced halocline after 40 years of coupled simulation (solid orange line). Furthermore, a maximum of about 34.69 g/kg develops, similar to the observed profiles, though substantially deeper and less confined, while a substantially higher salinity than observed establishes at depth. TP6M-T63.40 features less realistic results (solid dark blue line) as there is a much less pronounced halocline. TP6M-T63.90 shows a somewhat improved salinity profile (solid light blue line), though not to the extent of

TP6M-T255.40. For the wider WS (Fig. 9 middle panel), the finding is similar. On the larger scale (Fig. 9 bottom middle) it also seems that TP6M-T255.40 delivers the most realistic profile shape.

The stratification is ultimately indicated by the vertical density distribution (Fig. 9 right column). The reference pressure for the density profiles is 0 dbar. At temperatures around the freezing point the summer bias of 0.2 g/kg in salinity translates to about 0.16 kg/m<sup>3</sup> in density (e.g., Talley et al., 2011), i.e. the observed surface density (solid black line) in the central WS should be around 1027.7 kg/m<sup>3</sup> in winter. Focusing first on the central WS, the NCEP-forced simulation yields a realistic density at depth, but there is no indication of any stratification. 60 years into the NCEP-forced integration, stratification develops, but only by deep water becoming too dense (not shown). Immediately upon cou-

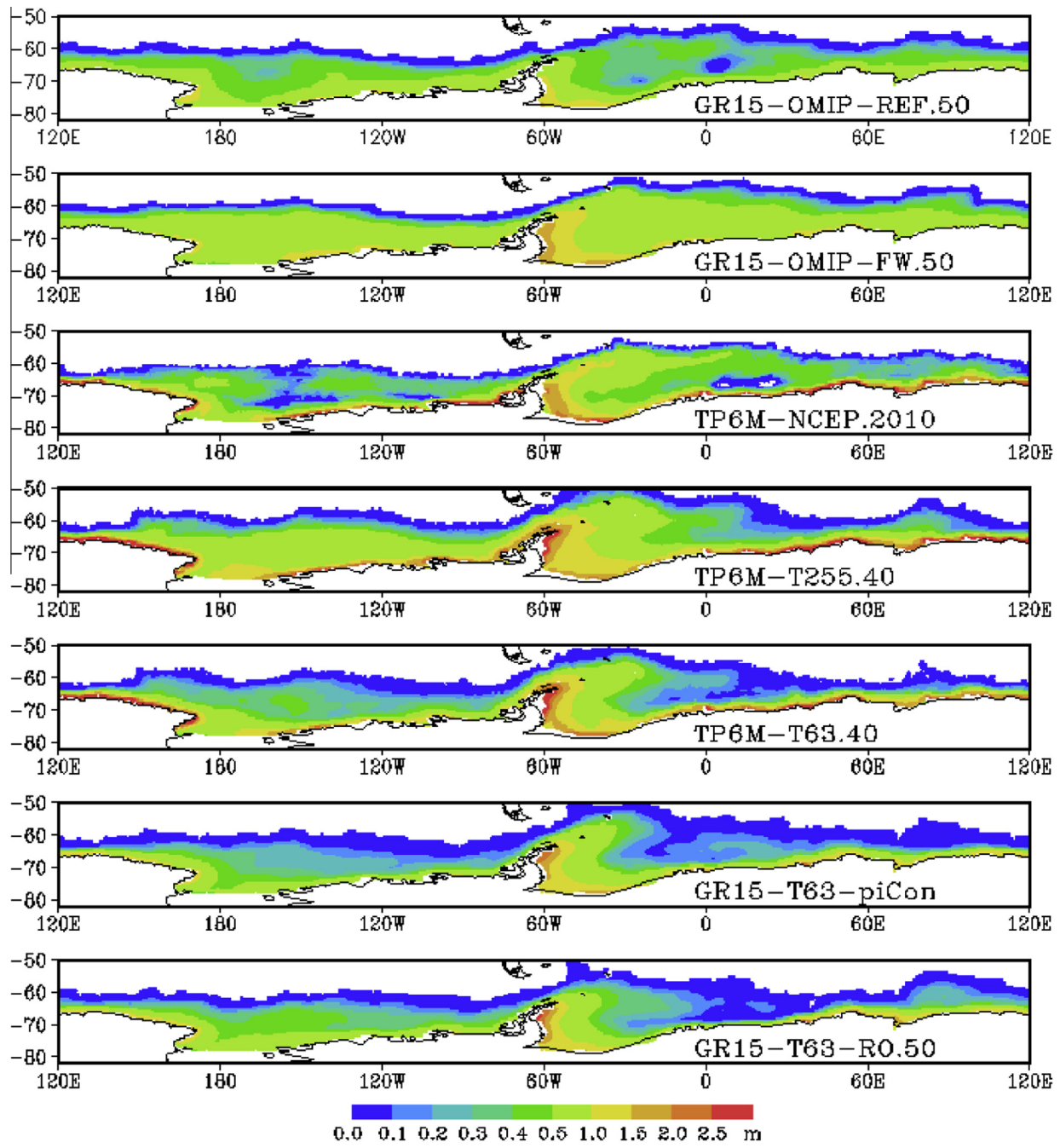


**Fig. 5.** 5-year August-mean sea-ice thickness for indicated experiments.

pling (TP6M-T255.0), the surface density diminishes (Fig. 9 top right, solid red line) in accord with salinity. 40 years into the coupled integration, density at depth returns to more realistic values (solid orange line). The upper layers experience a noticeable stratification in TP6M-T255.40, whereas that of TP6M-T63.40 is much less pronounced (solid dark blue line), and does only improve at depth after another 50 years of integration (solid light blue line). The tendencies are similar in the wider WS (Fig. 9 middle right), and apply in this case also to the circumpolar belt (Fig. 9 bottom right).

The dashed lines in Fig. 9 (dark green versus light green) illustrate the impact of the additional freshwater flux in the forced GR15 experiments. In the central WS (Fig. 9 top row), GR15-OMIP-FW.50 improves the density profile considerably, in particu-

lar in the upper 500 m. The salinity profile of GR15-OMIP-FW.50 is the most realistic of all experiments. The only noticeable difference to the observed profile is the location of the salinity maximum, which is located at 800 m depth, as opposed to 300 m in the observation. The ultimate improvement is found in the temperature profile. Similar improvements are apparent in the wider WS (Fig. 9 middle row) and in the circumpolar belt (Fig. 9 bottom row).

#### 4. Discussion

Having so far mostly concentrated on individual variables, we will now move on to discuss in more detail the inter-relationship between the variables. We start with an analysis of the factors that

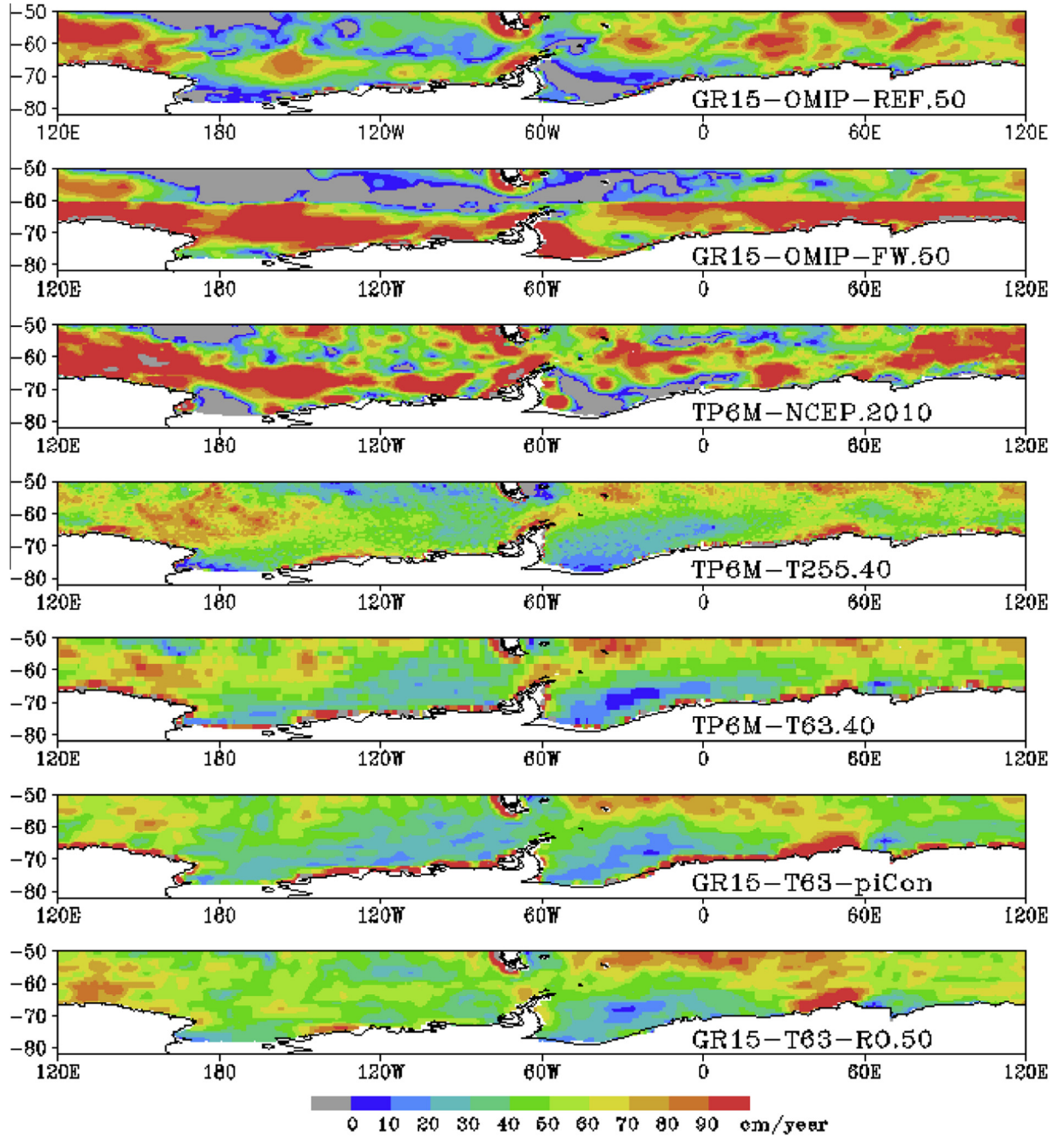


**Fig. 6.** Annual-mean external freshwater flux for indicated experiments.

influence sea-ice thickness. We find that the deep warm water reservoir and the amount of vertical mixing readily affect the sea-ice thickness, as illustrated in Fig. 5. At the end of the forced TP6M experiment and at the beginning of the coupled experiments, large areas are covered by sea ice, even those that feature excessive mixed-layer depths (Fig. 2). This is due to the fact that in these simulations the water column does not contain water that is noticeably warmer than the freezing point, i.e. excessive convection will not affect sea ice. After 40 years of coupled integration with the high-resolution AGCM (TP6M-T255.40), the sea-ice cover and thickness show a substantial increase (Fig. 5) even though the deep-ocean accumulated a considerable heat reservoir (Fig. 9 left column). The increase in sea-ice extent and thickness is thus due to a substantial reduction in vertical mixing, as reflected by a

reduced mixed-layer depth (Fig. 11) and by the stronger stratification (Fig. 9 right column). While the coupled simulation with the coarser AGCM (TP6M-T63) led to a similar build-up of a heat reservoir in the deep ocean, the mixed-layer thickness (not shown), even though somewhat reduced, remains excessive and is still affecting wide regions 40 years into the coupled integration. Accordingly, the stratification is weaker such that the sea ice can more readily be influenced by oceanic heat flux. Fig. 5 demonstrates that this goes to the point where open-ocean polynyas start emerging. Thus, the higher resolution AGCM produces surface conditions that trigger a stronger stratification.

In the following we shed more light on these relationships by examining in more detail why the SO performance of TP6M improved upon coupling with ECHAM6, and that of GR15-OMIP

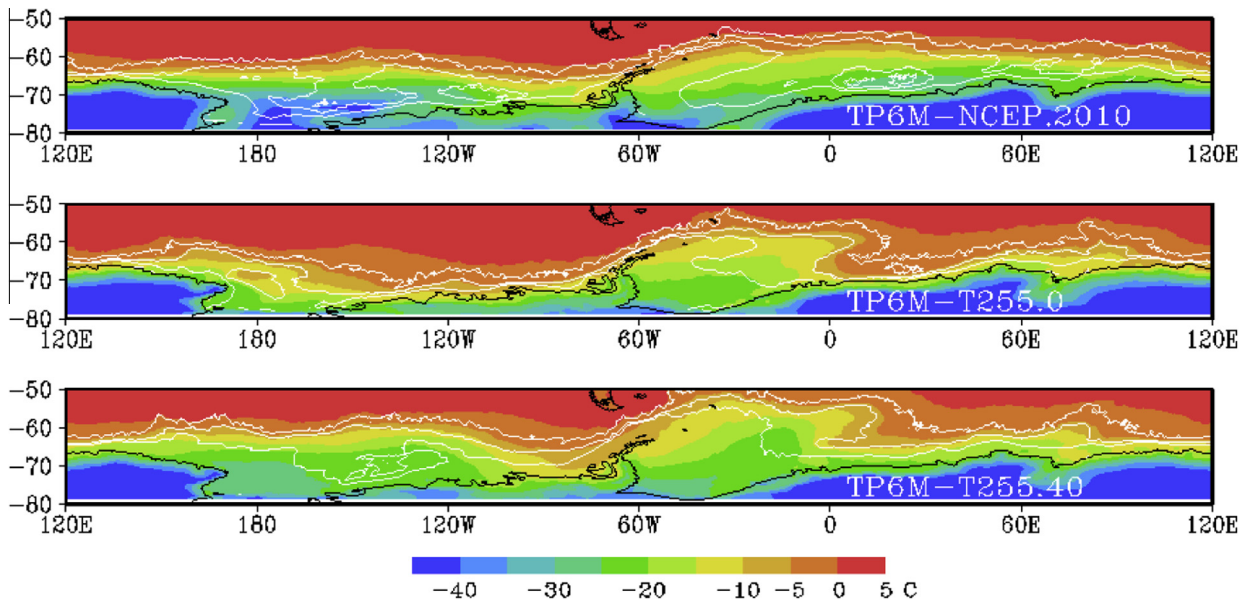


**Fig. 7.** August-mean 2-m air temperature (color) and sea-ice thickness (white lines, increment: 0.3 m, range: 0–0.6 m) for indicated experiments.

upon increasing the external freshwater flux. Both simulations end up with a substantially more realistic strength of the ACC due to more realistic density south of the ACC. The improved ACC in the forced GR15 experiments is exclusively caused by the enhanced external freshwater flux. The ice cover and the ACC improving in concert with the HLSO water masses strongly suggests that the additional freshwater flux is crucial for improving the model representation of the HLSO in MPIOM. Considering further that the observed temperature and salinity profiles reflect a rather complex water-mass distribution, maintaining it in a 50-year integration is remarkable. GR15-OMIP-FW.50 also yields a substantial increase in deep-ocean salinity, and a substantial salinity decrease in the upper 200 m, both changes leading to a rather realistic salinity profile. This indicates a switch in the mode of operation from open-ocean deep convection to no convection (e.g., Gordon et al., 2007; Martin et al., 2013), i.e., as long as there is convection, any freshening of the surface leads to a freshening of the deep-ocean. Beyond a certain threshold of surface freshening, stratification becomes strong enough to inhibit deep convection, which then results in an immediate build-up of a heat and salt reservoir at depth, i.e. CDW, which is ultimately maintained by the outflow of NADW (e.g., Pierce et al., 1995; Stössel and Kim, 2001).

The physical mechanism behind the direct relationship between freshwater supply in the HLSO and HLSO density (below 200 m) seems to occur in two steps. First, surface freshening increases the stratification, thus reducing the amount of dense-water formation through open-ocean convection. This allows for the buildup of warm and saline CDW at intermediate depths. At the same time, sea ice grows thicker and more compact (Fig. 5), which reduces surface heat loss in winter. This reduces ice growth and thus the amount of brine release, which in turn reduces the amount of oceanic heat flux affecting sea ice, until a subtle balance establishes between a considerable heat reservoir at depth and a reasonably thick and compact ice cover at the surface that inhibits the production of excessively dense deep water by open-ocean convection. There is an obvious increase of ice thickness and extent with an increase in external freshwater supply, and correspondingly a considerable decrease in surface heat loss.

A similar change is noticed with the TP6M experiments when switching from uncoupled to coupled mode, and when continuing the model integration in coupled mode. During the 40 years of

both coupled TP6M integrations, the strength of the ACC experiences a considerable decrease toward observed estimates (Table 1; Fig. 3). Besides changes in the external freshwater flux, this change can in the coupled case also be due to a decrease in the strength of the southern hemisphere westerlies from NCEP values to the ones provided by ECHAM6. Fig. 12 shows the meridional distribution of 6-year-mean zonal-mean zonal wind stress over the ocean south of 50°S for selected experiments (color) and observed climatologies/reanalyses (black). Switching from NCEP.2010 to TP6M-T255.40 is associated with a substantial reduction of westerly wind stress and with a northward shift of its core, both of which may readily explain the reduction of the ACC (e.g., Fyfe et al., 2007). Another aspect related to convection in the HLSO is the strength of the WS and RS gyre circulation, which is largely determined by the differential Ekman transport and thus the wind-stress curl. A steeper meridional gradient in zonal wind stress, such as NCEP relative to TP6M-T255 (Fig. 12), will lead to a stronger WS gyre, which in turn will lead to doming of isopycnals in its center and thus a more favorable environment for open-ocean convection. This mechanism has also been proposed in Cheon et al. (2014) who relate this to the occurrence of the WS polynya in the 1970s. A more negative wind-stress curl, as e.g. associated with a steepening of the zonal wind-stress curves in Fig. 12 would therefore promote open-ocean convection, a depletion of the heat reservoir at depth, an increase of HLSO subsurface density, and thus eventually lead to an increase in ACC strength.

Accordingly, Table 1 also shows the 6-year mean wind-stress curl over the ocean region south of 50°S. For the experiments discussed so far there is a clear relationship between the slopes in Fig. 12 and the magnitude of negative wind-stress curl. TP6M-NCEP.2010 clearly shows the largest negative wind-stress curl ( $-1.68 \cdot 10^{-7}$  Pa/m) and also the largest ACC strength. Immediately upon coupling, the curl diminishes to  $-1.27 \cdot 10^{-7}$  Pa/m and seemingly stays at that value over the next 40 years of coupled integration. The decrease of the ACC from 230 Sv to 141 Sv could thus be entirely due to the combined effect of reduced zonal wind stress and reduced wind-stress curl. This is particularly supported by the fact that the total external freshwater flux south of 60°S decreases upon coupling, thus promoting the preconditioning for convection. On the other hand, if the freshwater flux south of 70°S is decisive (see Section 3), its near doubling and presumed

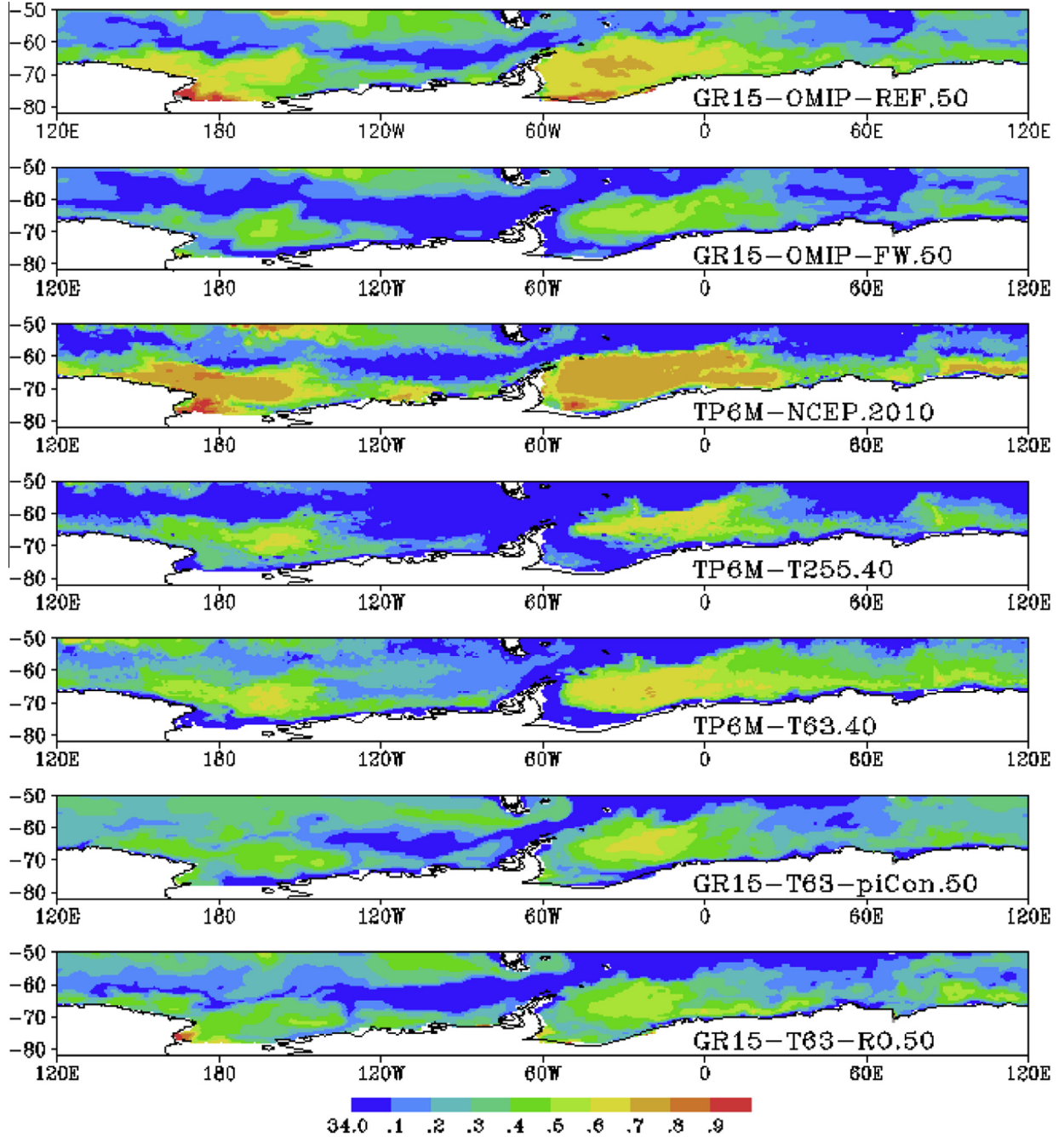


**Fig. 8.** August-mean uppermost model layer salinity for indicated experiments.

northward advection will contribute to reduced convection. In any case, the coupled simulations experience a considerable decrease of water density below 200 m south of the ACC (Fig. 4 and Table 1), which leads to a major reduction of the meridional density gradient across the ACC, and thus a weakening of the ACC itself. It is important to note that this dramatic reduction is seemingly just due to changes in the surface boundary conditions of the HLSO, i.e. reduction in zonal wind stress and magnitude of negative wind-stress curl, surface freshening, and warming upon coupling. All factors enhance the stratification of the ocean, reducing upward oceanic heat flux (e.g., Bitz et al., 2005; Zhang, 2007; Goosse et al., 2009; Kirkman and Bitz, 2011; Martin et al., 2013), allowing the buildup of thicker ice (Fig. 4) and a heat reservoir at depth (Fig. 9 left column). Fig. 10 shows the meridional winter sections along

30°W of GR15-OMIP-FW.50 corresponding to Figs. 1 and 2. The simulated vertical-meridional water-mass distribution of this forced experiment is in close agreement with the corresponding WOCE section (Fig. 1), even in absolute values. TP6M-T255.40 shows a similar distribution (Fig. 11), but with much colder water below 2000 m depth. This is likely due to the deep part of the HLSO not having adjusted after 40 years of coupled integration, as demonstrated for TP6M-T63.90 (Fig. 9 left column, solid light blue line).

This study is only to examine the short-term ( $\sim 50$  years), transient response of the HLSO to varying surface boundary conditions. As can be seen when going from TP6M-T63.40 to TP6M-T63.90, 50 years is not sufficient time for the regional baroclinic part of the circulation of the SO to adjust. Long-term impacts in association with the global overturning circulation were not considered.

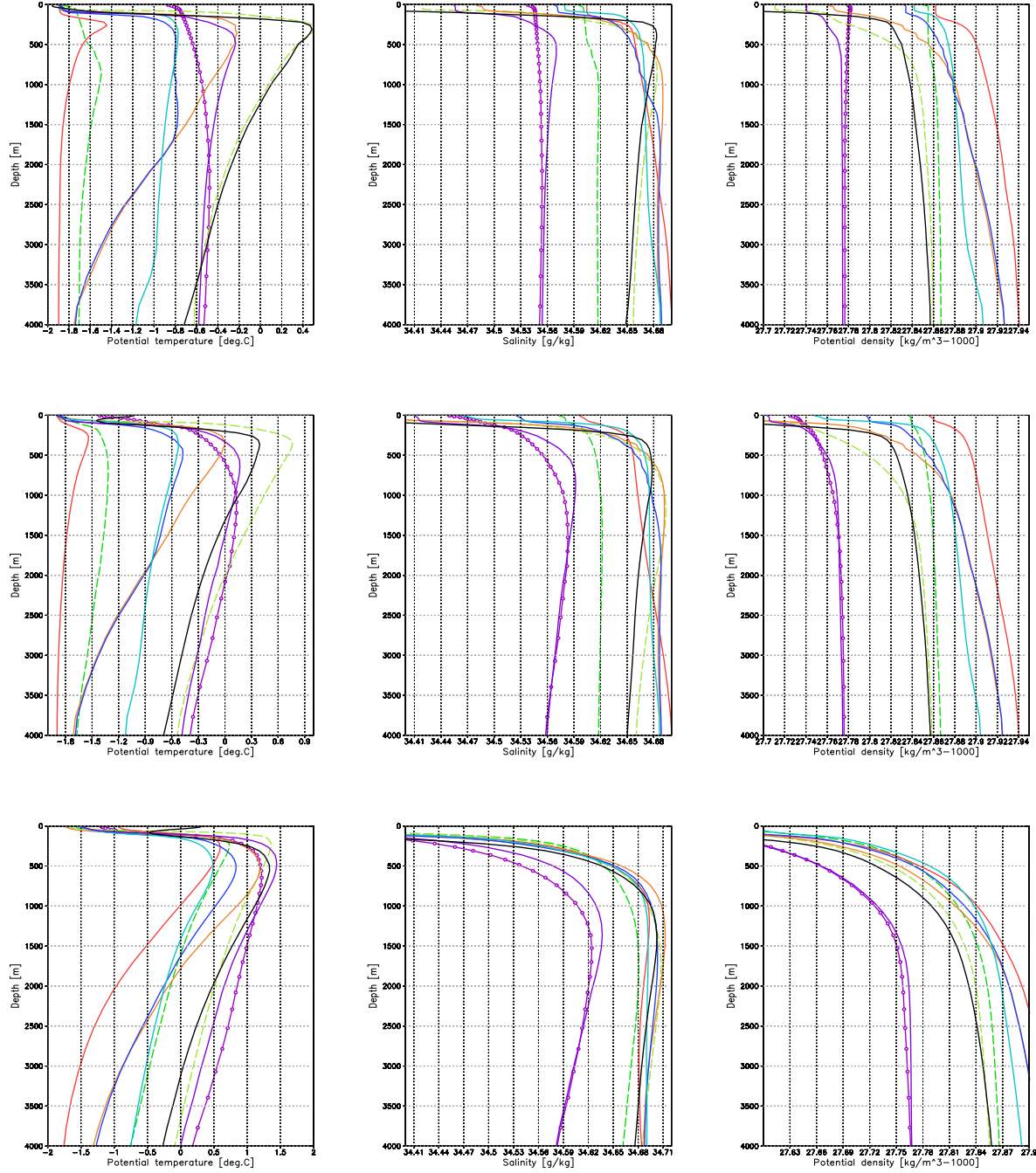


**Fig. 9.** Potential-temperature (left), salinity (middle), and potential-density (right) profiles at 30°W, 65°S (top), in region 20–40°W, 60–70°S (middle), in region 0–360°E, 60–70°S (bottom) from WOCE climatology (solid black), from uncoupled GR15-OMIP experiments (colored dashed lines) REF.50 (dark green), FW.50 (light green), and from coupled experiments (colored solid lines) TP6M-T255.0 (red), TP6M-T255.40 (orange), TP6M-T63.40 (dark blue), TP6M-T63.90 (light blue), GR15-T63-RO.50 (purple), and GR15-T63-piCon (purple with symbols). All simulation results reflect August-mean conditions. (For interpretation of the references to colour in this figure legend, the reader is referred to the web version of this article.)

On a time scale of several hundred years, the HLSO will be affected by the global circulation, in particular by the properties and the rate of NADW outflow (e.g., Pierce et al., 1995; Drijfhout et al., 1996; Stössel et al., 2002; Martin et al., 2013). The long-term impact emerges in the HLSO properties of the preindustrial control simulation of CMIP5, e.g. MPI-ESM-LR. This coupled simulation (in the current setting named GR15-T63-piCon) shows some improvement over TP6M-NCEP.2010 (Fig. 2), e.g. the existence of a substantial heat reservoir in the central WS gyre (Fig. 9 left column, marked purple line). In combination with excessive convection, however, this yields much thinner ice than in the forced case to

the point that open-ocean polynyas emerge (Fig. 5). Furthermore, the deep ocean salinity of the central WS gyre is substantially underestimated, with a concomitant underestimation of density (Fig. 9 middle and right column, marked purple lines). This misrepresentation is also evident from Table 1, GR15-T63-piCon showing the lowest HLSO density of all listed experiments, while the external freshwater flux into the HLSO is lower than that of the TP6M coupled experiments. On the other hand, the strength of the ACC turns out to be on the high side. From Table 1 and Fig. 12 it is also evident that the stronger ACC cannot be explained by differences in zonal wind stress and wind-stress curl. In this context it is interest-

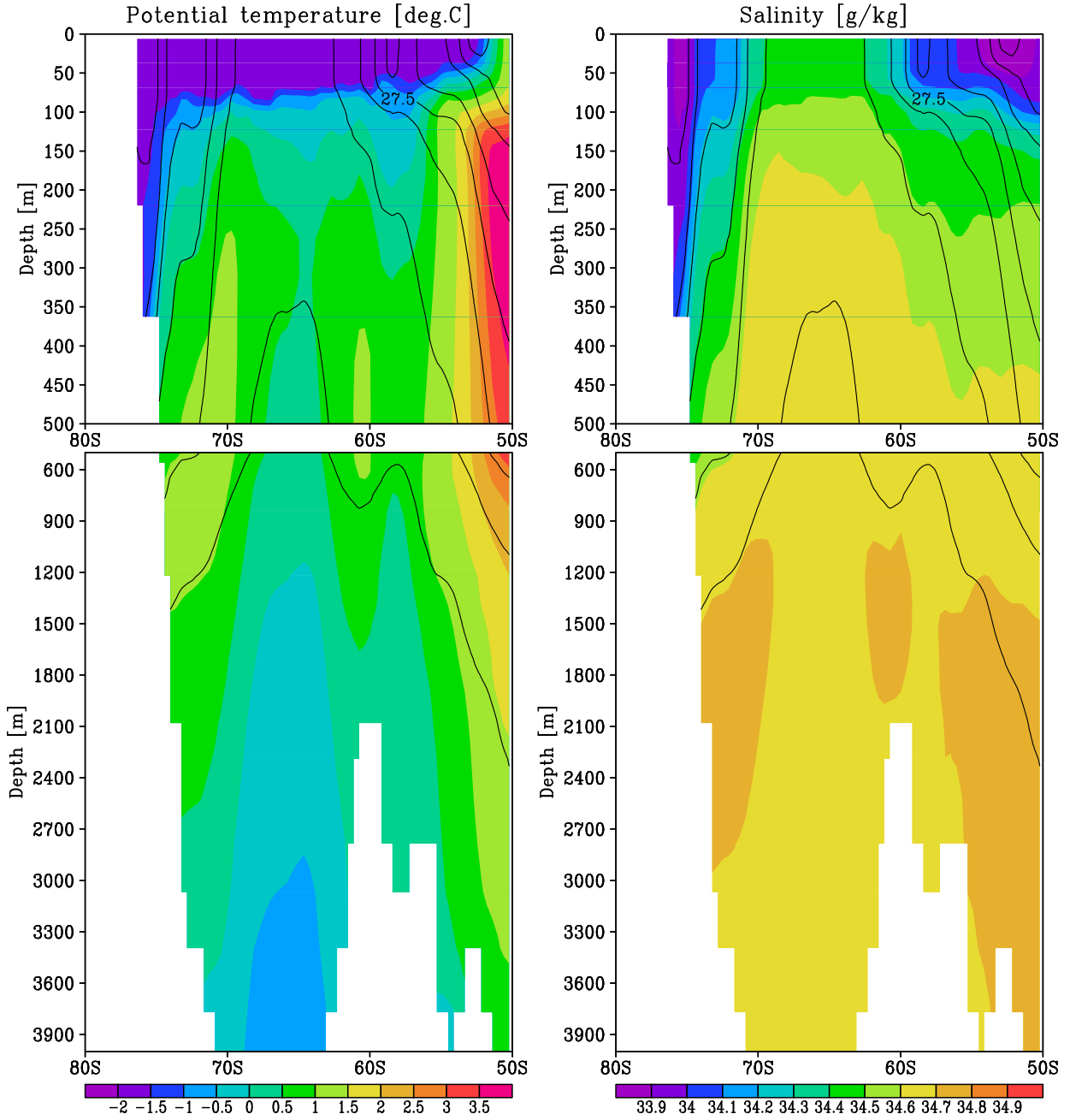


**Fig. 10.** Results from GR15-OMIP-FW.50; otherwise as Fig. 2.

ing to note that the HLSO of the coupled simulation of the corresponding NCAR model (CCSM4) is too salty by about 0.2 g/kg (Weijer et al., 2012), with a concomitant excessive ACC strength of 173 Sv which seems to be mainly due to an excessive westerly wind stress of up 0.21 N/m<sup>2</sup> (Meijers et al., 2012).

A problem with the improved open-ocean water-mass characteristics in the HLSO of the forced experiments is that the rate of AABW formation slows down to unacceptable values (e.g., decrease of AABW intrusion into Atlantic from about 4 Sv to 1 Sv in GR15-OMIP-FW.50). A similar reduction of AABW intrusion occurs in the coupled TP6M simulations, though from 9 Sv to 5 Sv, which is acceptable (e.g., Ganachaud and Wunsch, 2000; Sloyan and Rintoul, 2001). In these simulations, sea-ice thickness is overestimated along most of the Antarctic coastline, in particular along east Antarctica, and coincides with large local freshwater input

through runoff. Excessive runoff may stabilize the water column to the point that not enough AABW is being produced through the process of near-boundary convection. Considering that glacial melt water spreads to a large extent through icebergs (e.g., Gladstone et al., 2001), it seems sensible and physically justified to distribute part of the runoff from Antarctica over the HLSO, instead of dumping it all into coastal grid cells. Such measure should suppress open-ocean convection and simultaneously enhance near-boundary convection (e.g., Martin and Adcroft, 2010). To mimic this effect in a most simplistic way, we conducted a sensitivity experiment with the coupled GR15-T63 (MPI-ESM-LR) model starting from the preindustrial control year 1850, and assuming that all Antarctic runoff (glacial meltwater) normally entering the coastal ocean grid cells be distributed evenly over the ocean region south of 60°S, thereby conserving freshwater. This

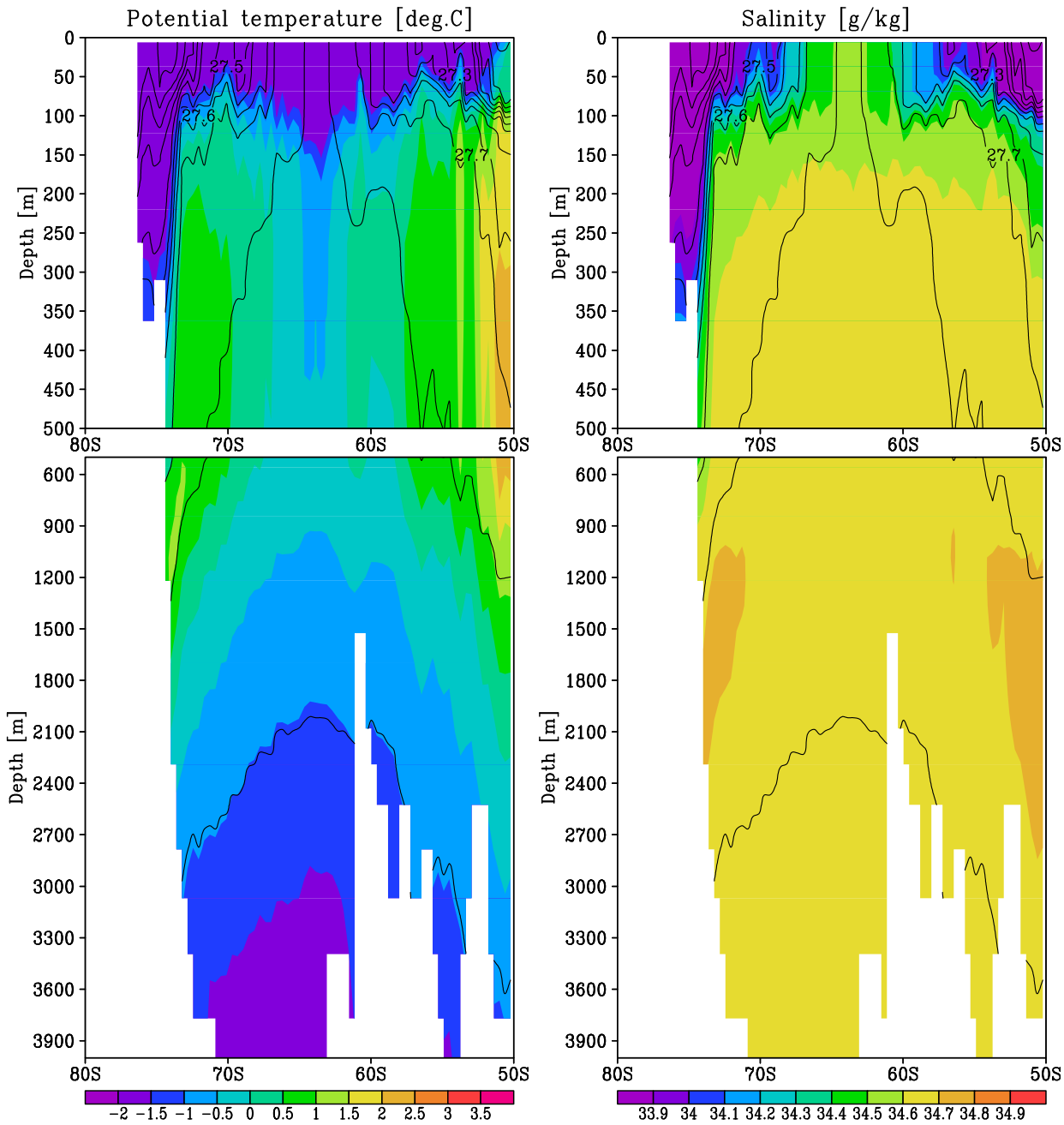


**Fig. 11.** Results from TP6M-T255.40; otherwise as Fig. 2.

provides an upper bound estimate of the effect of iceberg drift, as in reality about half of the glacial melt water still enters the ocean right at the coast in the form of basal melt water (Depoorter et al., 2013).

The results are shown under GR15-T63-RO.50 in Table 1 and in most of the figures. As expected, the total external freshwater flux south of 70°S (Table 1) and generally along the coast (Fig. 6) diminishes relative to GR15-T63-piCon (which would be the reference case for this set of experiments), while the freshwater flux south of 60°S remains approximately the same. Associated with the reduced freshwater flux south of 70°S is a higher sea-surface salinity (Fig. 8). The difference in coastal salinity is about 0.3 g/kg and extends down to about 300 m depth (not shown). Accordingly, the density along the coast increases to much more realistic values

(Table 1, Fig. 4), suggesting that sea-ice formation and AABW formation along the coast have improved. The larger high-latitude density may partly explain the stronger ACC (from 160 Sv to 178 Sv) (Table 1; Fig. 3) following our earlier explanation. Furthermore, the sea level in the central WS declined by 3 cm, and the horizontal volume-transport streamfunction of the WS increased by 2%, in line with the enhanced negative wind-stress curl over the HLSO (Table 1, Fig. 12). While the stronger ACC strength is less realistic compared to GR15-T63-piCon, there is a slight improvement of the HLSO water-mass properties between 60°S and 70°S and in the central WS (Fig. 9 from marked purple profiles to plain solid purple profiles), indicating that a longer integration may eventually lead to more realistic HLSO properties. The major improvement occurring along the coast suggests that it is rather

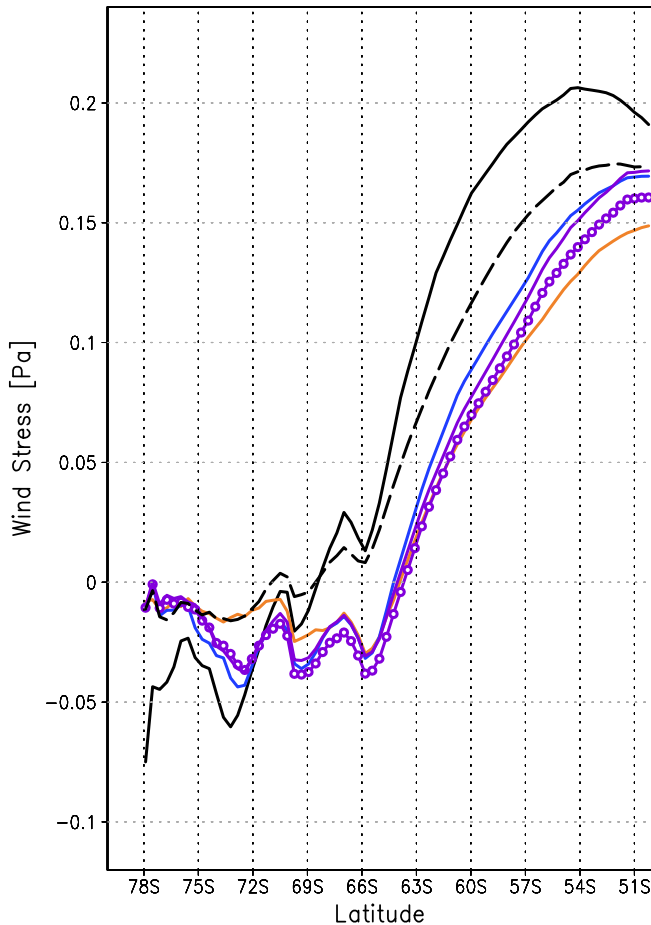


**Fig. 12.** 6-year-mean, zonal-mean wind stress from coupled experiments (colored solid lines) TP6M-T255.40 (orange), TP6M-T63.40 (dark blue), GR15-T63-RO.50 (purple), and GR15-T63-piCon.50 (purple with symbols), as well as year 2010 NCEP (solid black) and OMIP (dashed black). (For interpretation of the references to colour in this figure legend, the reader is referred to the web version of this article.)

the reduction of freshwater flux along the coast that leads to improvements than its increase further offshore, quite in line with the findings of [Martin and Adcroft \(2010\)](#).

## 5. Summary and conclusions

It can generally be concluded that MPIOM is capable of simulating the presently observed (e.g., [Gordon et al., 2007](#)) complex water-mass structure of the central WS provided the surface fluxes are such that they prevent open-ocean deep convection. A prerequisite for a realistic simulation is sufficient external freshwater input through precipitation or glacial melt water (e.g., [Marsland and Wolff, 2001](#)), a realistic westerly wind stress and wind-stress curl over the HLSO, and/or a more realistic redistribution of freshwater by sea ice. Observed estimates on the amount and distribution of glacial melt water bear large uncertainties (e.g., [Gladstone et al., 2001](#); [Beckmann and Goosse, 2003](#); [da Silva et al., 2006](#); [Jongma et al., 2009](#); [Tournadre et al., 2012](#); [Depoorter et al., 2013](#)). Distributed over the ocean area south of 60°S, these estimates convert to about 10 cm/year ([Table 1](#)). Over the same area, the net annual freshwater flux due to precipitation from reanalyses ranges from 60 to 70 cm/year (e.g., [Bromwich et al., 2011](#)). Evaporation rates from reanalyses in this region seem more inconsistent, probably due to differences in the way sea-ice concentration and -thickness are being prescribed. We estimate the mean evaporation rate to be around 10 cm/year (e.g., [Källberg et al., 2005](#)), thus

roughly compensating the estimated glacial melt water input to this region. Accordingly, the total external freshwater flux of GR15-OMIP-FW.50 ([Table 1](#)) is overestimated by about 22 cm/year. A problem with this simulation is that it is uncoupled so that buoyancy loss due to negative sensible heat flux in wintertime is exaggerated. In order to arrive at reasonable HLSO water-mass properties, this can apparently be compensated by buoyancy gain from extra freshwater flux.

Forced model experiments with the Large-Scale Geostrophic model (LSG) ([Pierce et al., 1995](#)) suggest that a freshwater input south of 60°S of about 82 cm/year is needed to support regime shifts from a HLSO convective to non-convective mode of operation, and vice versa. [Martin et al. \(2013\)](#), employing the coupled ECHAM5-NEMO model, achieve this with a freshwater input of only about 47 cm/year (apparently, this value of precipitation minus evaporation includes glacial melt/continental runoff). As can be seen from [Table 1](#), the HLSO freshwater flux value of [Pierce et al. \(1995\)](#) corresponds to our uncoupled experiment GR15-OMIP-FW.50, whereas the lower value of [Martin et al. \(2013\)](#) is closer to those of our coupled experiments TP6M-T255 and TP6M-T63. These experiments showing substantial improvements of HLSO water-mass properties in comparison with TP6M-NCEP.2010, an addition of 10 cm/year south of 60°S from about 55 cm/year to observed estimates of about 65 cm/year in the coupled TP6M experiments will likely be sufficient for shutting down open-ocean convection. This is somewhat counterintuitive as TP6M-NCEP.2010 has apparently more realistic external freshwater flux values than any of the coupled TP6M experiments, but then it features also the strongest westerly wind stress and strongest negative wind-stress curl.

An issue not analyzed in this study is the internal freshwater flux, i.e. that associated with the annual rate and pattern of seawater freezing and sea-ice melting (e.g., [Bitz et al., 2005](#); [Kirkman and Bitz, 2011](#)). Wind field errors will have a direct impact on sea-ice drift and the pattern and rate of annual net freezing (e.g., [Holland and Kwok, 2012](#); [Close and Goosse, 2013](#); [Turner et al., 2013](#); [Holland et al., 2014](#)). Another uncertainty arises from the way sea-ice salinity is being treated. In MPIOM, it is fixed at a value of 5 g/kg. This is at the low end of possible values for first-year ice (e.g., [Vancoppenolle et al., 2009](#); [Hunke et al., 2011](#)), which is the dominant ice type in the SO. A higher sea-ice salinity of about 8 g/kg would diminish brine release during sea formation, and thus deliver a stabilizing buoyancy flux in fall and winter in the open ocean, but also along the coast. In any case, insufficient sea-ice export from the coastal regions will contribute to underestimating near-boundary convection and to overestimating open-ocean convection. This role of the sea-ice induced freshwater flux is currently being investigated based on satellite data (Haumann, pers. comm., 2014).

With respect to the question of whether using a higher-resolution (and thus substantially more expensive) atmosphere model in coupled simulations delivers more realistic results in the HLSO the answer based on this study is yes. TP6M-T255 delivers more realistic winter sea ice and water-mass properties than TP6M-T63, while the ACC strength is equally well represented. Considering that the coupling frequency is identical, differences are solely due to horizontal resolution. Pronounced differences between TP6M-T255 and TP6M-T63 occur in wind stress right along Antarctica, in particular along Victoria Land (165°E), which is orographically the extension of the Transantarctic Mountain range. These differences resemble those found by [Stössel et al. \(2011\)](#) in this region. They compared T799 (i.e. about 20 km) resolution wind fields from the ECMWF operational analysis with those of the NCEP reanalyses, which have a resolution of about 200 km (about T63) in this region. A more detailed resolution of the coastal winds is crucial for the model representation of coastal polynyas and thus the

rate of AABW formation through near-boundary convection. The reasons for discrepancies related to the resolution of atmospheric fields will be the subject of further investigations.

As shown in this study, and consistent to earlier findings, the main players controlling the HLSO properties are the amount and distribution of the freshwater flux, and the strength and meridional gradient of the southern hemisphere westerlies. Continuing a forced eddy-resolving ocean simulation in coupled mode improves the HLSO properties considerably, at least over a time span of 40 years. Increased resolution of the atmosphere model leads to further improvements. The Antarctic runoff of the coupled simulations appears too concentrated along coastal grid points. Relaxing this situation by distributing this runoff over a wider region improves the HLSO water-mass properties, in particular along the coastline. This contributes to a more realistic representation of AABW formation through near-boundary convection, while the effect on open-ocean convection seems minor.

Recent literature on the performance of the HLSO focused on intercomparisons among CMIP5 models (e.g., Russell et al., 2006; Meijers et al., 2012; Zunz et al., 2013; Close and Goosse, 2013; Heuzé et al., 2013; Sallée et al., 2013; Turner et al., 2013). This study suggests that it may be worth scrutinizing the HLSO performance of individual ESMs under various conditions (model resolution, parameterizations, forced vs. coupled, initial conditions, glacial meltwater, transient vs. equilibrium conditions) to eventually arrive at more realistic simulations and a better understanding of this highly dynamic and complex region of the world's ocean.

## Acknowledgments

Thanks are due to Jin-Song v. Storch, Stephan Lorenz, and Stephanie Legutke for fruitful discussions and suggestions on this research. Furthermore, we thank Irina Fast for providing links and information on some of the data files that were analyzed. Thanks are also due to 2 anonymous reviewers for their valuable comments on the manuscript. The first author was funded through stipends from the Max Planck Society while on faculty development leave from Texas A&M University and during summer terms. F.A.H. is supported by ETH Research Grant CH2-01 11-1.

## References

- Adcroft, A., Hill, C., Marshall, J., 1997. Representation of topography by shaved cells in a height coordinate ocean model. *Mon. Weather Rev.* 125, 2293–2315.
- Beckmann, A., Goosse, H., 2003. A parameterization of ice shelf-ocean interaction for climate models. *Ocean Model.* 5, 157–170.
- Bintanja, R., van Oldenborgh, G.J., Drijfhout, S.S., Wouters, B., Katsman, C.A., 2013. Important role for ocean warming and increased ice-shelf melt in Antarctic sea-ice expansion. *Nat. Geosci.* 6, 376–379.
- Bitz, C.M., Holland, M.M., Hunke, E.C., Moritz, R.E., 2005. Maintenance of the sea-ice edge. *J. Clim.* 18, 2903–2921.
- Bromwich, D.H., Nicolas, J.P., Monaghan, A.J., 2011. An assessment of precipitation changes over Antarctica and the Southern Ocean since 1989 in contemporary global reanalyses. *J. Clim.* 24, 4189–4209.
- Carmack, E.C., 1990. Large-scale physical oceanography of polar oceans. In: *Polar Oceanography, Part A: Physical Science*. Academic Press, pp. 171–222.
- Cheon, W.G., Stössel, A., 2009. Oceanic response to interactive momentum flux over southern hemisphere sea ice. *J. Geophys. Res.* 114, C12002. <http://dx.doi.org/10.1029/2008JC005068>.
- Cheon, W.G., Park, Y.G., Toggweiler, J.R., Lee, S.K., 2014. The relationship of Weddell polynya and open-ocean deep convection to the southern hemisphere westerlies. *J. Phys. Oceanogr.* 44, 694–713.
- Close, S.E., Goosse, H., 2013. Entrainment-driven modulation of Southern Ocean mixed layer properties and sea ice variability in CMIP5 models. *J. Geophys. Res.* 118, 2811–2827.
- Cunningham, S.A., Alderson, S.G., King, B.A., Brandon, M.A., 2003. Transport and variability of the Antarctic circumpolar current in drake passage. *J. Geophys. Res.* 108, C58084. <http://dx.doi.org/10.1029/2001JC001147>.
- de Lavergne, C., Palter, J.B., Galbraith, E.D., Bernardello, R., Marinova, I., 2014. Cessation of deep convection in the open Southern Ocean under anthropogenic climate change. *Nat. Clim. Change* 4, 278–282. <http://dx.doi.org/10.1038/nclimate2132>.
- Depoorter, M.A., Bamber, J.L., Griggs, J.A., Lenaerts, J.T.M., Ligtenberg, S.R.M., van den Broeke, M.R., Moholdt, G., 2013. Calving fluxes and basal melt rates of Antarctic ice shelves. *Nature* 12567 (10.1038).
- Drijfhout, S.S., Heinze, C., Latif, M., Maier-Reimer, E., 1996. Mean circulation and internal variability in an ocean primitive equation model. *J. Phys. Oceanogr.* 26, 559–580.
- Fyfe, J.C., Saenko, O.A., Zickfeld, K., Eby, M., Weaver, A.J., 2007. The role of poleward-intensifying winds on Southern Ocean warming. *J. Clim.* 20, 5391–5400.
- Ganachaud, A., Wunsch, C., 2000. Improved estimates of global ocean circulation, heat transport and mixing from hydrographic data. *Nature* 408, 453–456.
- Gladstone, R.M., Bigg, G.R., Nicholls, K.W., 2001. Iceberg trajectory modeling and meltwater injection in the Southern Ocean. *J. Geophys. Res.* 106, 19903–19915.
- Goosse, H., Lefebvre, W., de Montety, A., Crespin, E., Orsi, A.H., 2009. Consistent past half-century trends in the atmosphere, the sea ice and the ocean at high southern latitudes. *Clim. Dyn.* 33, 999–1016. <http://dx.doi.org/10.1007/s00382-008-0500-9>.
- Gordon, A.L., 2014. Southern Ocean polynya. *Nat. Clim. Change* 4, 249–250.
- Gordon, A.L., Huber, B.A., 1990. Southern Ocean winter mixed layer. *J. Geophys. Res.* 95, 11655–11672.
- Gordon, A.L., Visbeck, M., Comiso, J.C., 2007. A possible link between the Weddell polynya and the southern annular mode. *J. Clim.* 20, 2558–2571.
- Griffies, S.M. et al., 2009. Coordinated ocean-ice reference experiments (COREs). *Ocean Modell.* 26, 1–46.
- Hall, M.M., McCartney, M., Whitehead, J.A., 1997. Antarctic bottom water flux in the equatorial Western Atlantic. *J. Phys. Oceanogr.* 27, 1903–1926.
- Haumann, F.A., Notz, D., Schmidt, H., 2014. Anthropogenic influence on recent circulation-driven Antarctic sea-ice changes. *Geophys. Res. Lett.* <http://dx.doi.org/10.1002/2014GL061659>.
- Heuzé, C., Heywood, K.J., Stevens, D.P., Ridley, J.K., 2013. Southern Ocean bottom water characteristics in CMIP5 models. *Geophys. Res. Lett.* 40, 1409–1414.
- Hogg, N.G., Zenk, W., 1997. Long-period changes in the bottom water flowing through Vema Channel. *J. Geophys. Res.* 102, 15,639–15,646.
- Holland, P.R., Kwok, R., 2012. Wind-driven trends in Antarctic sea-ice drift. *Nat. Geosci.* 5, 872–875.
- Holland, P.R., Bruneau, N., Enright, C., Losch, M., Kurtz, N.T., Kwok, R., 2014. Modeled trends in Antarctic sea ice thickness. *J. Clim.* 27, 3784–3801.
- Hunke, E.C., Notz, D., Turner, A.K., Vancoppenolle, M., 2011. The multiphase physics of sea ice: a review for model developers. *Cryosphere* 5, 989–1009.
- Jongma, J.I., Driesschaert, E., Fichefet, T., Goosse, H., Renssen, H., 2009. The effect of dynamic-thermodynamic icebergs on the Southern Ocean climate in a three-dimensional model. *Ocean Modell.* 26, 104–113.
- Jungclaus, J.H., Keenlyside, N., Botzet, M., Haak, H., Luo, J.J., Latif, M., Marotzke, J., Mikolajewicz, U., Roeckner, E., 2006. Ocean circulation and tropical variability in the coupled model ECHAM5/MPI-OM. *J. Clim.* 19, 3952–3972.
- Jungclaus, J.H., Fischer, N., Haak, H., Lohmann, K., Marotzke, J., Matei, D., Mikolajewicz, U., Notz, D., von Storch, J.S., 2013. Characteristics of the ocean simulations in the Max Planck Institute Ocean Model (MPIOM) the ocean component of the MPI-Earth system model. *J. Adv. Mod. Earth Syst.* 5, 422–446.
- Källberg, P., Berrisford, P., Hoskins, B., Simmons, A., Uppala, S., Lamy-Thépaut, S., Hines, R., 2005. ECMWF re-analysis. Project Report Series No. 19. ERA-40 Atlas.
- Kirkman IV, C.H., Bitz, C.M., 2011. Effect of the sea ice freshwater flux on Southern Ocean temperatures in CCSM3: deep-ocean warming and delayed surface warming. *JCL* 24, 2224–2237.
- Knutti, R., Sedláček, J., 2013. Robustness and uncertainties in the new CMIP5 climate model projections. *Nat. Clim. Change* 3, 369–373.
- Lemke, P., Ren, J., Alley, R.B., Allison, I., Carrasco, J., Flato, G., Fujii, Y., Kaser, G., Mote, P., Thomas, R.H., Zhang, T., 2007. Observations: changes in snow, ice and frozen ground. In: Solomon, S., Qin, D., Manning, M., Chen, Z., Marquis, M., Averyt, K.B., Tignor, M., Miller, H.L. (Eds.), *Climate Change 2007: The Physical Science Basis. Contribution of Working Group I to the Fourth Assessment Report of the Intergovernmental Panel on Climate Change*. Cambridge University Press, Cambridge, United Kingdom, New York, NY, USA.
- Maier-Reimer, E., Mikolajewicz, U., Hasselmann, K., 1993. Mean circulation of the Hamburg LSG OGCM and its sensitivity to the thermohaline surface forcing. *J. Phys. Oceanogr.* 23 (4), 731–757.
- Maksym, T., Markus, T., 2008. Antarctic sea ice thickness and snow-to-ice conversion from atmospheric reanalysis and passive microwave snow depth. *JGR* 113, C02S12. <http://dx.doi.org/10.1029/2006JC004085>.
- Maksym, T., Stammerjohn, S.E., Ackley, S., Massom, R., 2012. Antarctic sea ice – a polar opposite? *Oceanography* 25, 140–151.
- Marshall, J., Schott, F., 1999. Open-ocean convection: observations, theory, and models. *Rev. Geophys.* 37, 1–64.
- Marsland, S., Wolff, J.-O., 2001. On the sensitivity of Southern Ocean sea ice to the surface fresh-water flux: a model study. *J. Geophys. Res.* 106 (C2), 2723–2741.
- Martin, T., Adcroft, A., 2010. Parameterizing the fresh-water flux from land ice to ocean with interactive icebergs in a coupled climate model. *Ocean Modell.* 34, 111–124.
- Martin, T., Park, W., Latif, M., 2013. Multi-centennial variability controlled by Southern Ocean convection in the Kiel climate model. *Clim. Dyn.* 40, 2005–2022.
- Massonnet, F., Mathiot, P., Fichefet, T., Goosse, H., König-Beatty, C., Vancoppenolle, M., Lavergne, T., 2013. A model reconstruction of the Antarctic sea ice thickness and volume changes over 1980–2008 using data assimilation. *Ocean Modell.* 64, 67–75.

- Mathiot, P., Barnier, B., Gallée, H., Molines, J.M., Le Sommer, J., Juza, M., Penduff, T., 2010. Introducing katabatic winds in global ERA40 fields to simulate their impacts on the Southern Ocean and sea-ice. *Ocean Model.* 35, 146–160.
- Meehl, G.A., Stocker, T.F., Collins, W.D., Friedlingstein, P., Gaye, A.T., Gregory, J.M., Kitoh, A., Knutti, R., Murphy, J.M., Noda, A., Raper, S.C.B., Watterson, I.G., Weaver, A.J., Zhao, Z.C., 2007. Global climate projections. In: Solomon, S., Qin, D., Manning, M., Chen, Z., Marquis, M., Averyt, K.B., Tignor, M., Miller, H.L. (Eds.), *Climate Change 2007: The Physical Science Basis. Contribution of Working Group I to the Fourth Assessment Report of the Intergovernmental Panel on Climate Change*. Cambridge University Press, Cambridge, United Kingdom, New York, NY, USA.
- Meijers, A.J.S., Shuckburgh, E., Bruneau, N., Sallée, J.-B., Bracegirdle, T.J., Wang, Z., 2012. Representation of the Antarctic circumpolar current in the CMIP5 climate models and future changes under warming scenarios. *JGR* 117, C12008. <http://dx.doi.org/10.1029/2012JC008412>.
- Müller, M., Haak, H., Jungclaus, J.H., Sündermann, J., Thomas, M., 2010. The effect of ocean tides on a climate model simulation. *Ocean Model.* 35, 304–313.
- Notz, D., Haumann, F.A., Haak, H., Jungclaus, J.H., Marotzke, J., 2013. Arctic sea-ice evolution as modeled by Max Planck Institute for Meteorology's earth system model. *J. Adv. Mod. Earth Syst.* 5, 173–194.
- Oke, P.R., England, M.H., 2004. Oceanic response to changes in the latitude of the southern hemisphere subpolar westerly winds. *J. Clim.* 17, 1040–1054.
- Orsi, A.H., Johnson, G.C., Bullister, J.L., 1999. Circulation, mixing, and production of Antarctic bottom water. *Prog. Oceanogr.* 43, 55–109.
- Orsi, A.H., Whitworth III, T., 2005. Hydrographic atlas of the World Ocean circulation experiment (WOCE). In: Sparrow, M., Chapman, P., Gould, J. (Eds.), *Southern Ocean*, vol. 1. International WOCE Project Office, Southampton, UK, ISBN 0-904175-49-9.
- Park, W., Latif, M., 2008. Multidecadal and multicentennial variability of the meridional overturning circulation. *Geophys. Res. Lett.* 35, L22703.
- Parkinson, C.L., Cavalieri, D.J., 2012. Antarctic sea ice variability and trends, 1979–2010. *TCD* 6 (2), 931–956.
- Pierce, D.W., Barnett, T.P., Mikolajewicz, U., 1995. Competing roles of heat and freshwater flux in forcing thermohaline oscillations. *J. Phys. Oceanogr.* 25, 2046–2064.
- Powell, D.C., Markus, T., Stössel, A., 2005. Effects of snow depth forcing on Southern Ocean sea ice simulations. *J. Geophys. Res.* 110 (C6), C06001. <http://dx.doi.org/10.1029/2003JC002212>.
- Röske, F., 2006. A global heat and freshwater forcing dataset for ocean models. *Ocean Model.* 11, 197–235.
- Russell, J.L., Stouffer, R.J., Dixon, K.W., 2006. Intercomparison of the Southern Ocean circulations in IPCC coupled model control simulations. *J. Clim.* 19, 4560–4575.
- Sallée, J.-B., Shuckburgh, E., Bruneau, N., Meijers, A.J.S., Bracegirdle, T.J., Wang, Z., Roy, T., 2013. Assessment of Southern Ocean water mass circulation and characteristics in CMIP5 models: historical bias and forcing response. *J. Geophys. Res.* 118, 1830–1844.
- Silva, T.A.M., Bigg, G.R., Nicholls, K.W., 2006. Contribution of giant icebergs to the Southern Ocean freshwater flux. *J. Geophys. Res.* 111. <http://dx.doi.org/10.1029/2004JC002843>.
- Sloyan, B.M., Rintoul, S.R., 2001. The Southern Ocean limb of the global deep overturning circulation. *J. Phys. Oceanogr.* 31, 143–173.
- Sloyan, B.M., Kamenkovich, I.V., 2007. Simulation of subantarctic mode and intermediate waters in climate models. *J. Clim.* 20, 5061–5080.
- Stevens, B., Giorgetta, M., Esch, M., Mauritzen, T., Crucifix, T., Rast, S., Salzmann, M., Schmidt, H., Bader, J., Block, K., Brokopf, R., Fast, I., Kinne, S., Kornblueh, L., Lohmann, U., Pincus, R., Reichler, T., Roeckner, E., 2013. Atmospheric component of the MPI-M Earth System Model: ECHAM6. *J. Adv. Mod. Earth Syst.* 5, 1–27.
- Stössel, A., 2008. Employing satellite-derived sea-ice concentration to constrain upper-ocean temperature in a global ocean GCM. *J. Clim.* 21 (17), 4498–4513.
- Stössel, A., Kim, S.-J., 2001. Decadal deep-water variability in the subtropical Atlantic and convection in the Weddell Sea. *J. Geophys. Res.* 106 (C10), 22,425–22,440.
- Stössel, A., Yang, K., Kim, S.-J., 2002. On the role of sea ice and convection in a global ocean model. *J. Phys. Oceanogr.* 32, 1194–1208.
- Stössel, A., Zhang, Z., Vihma, T., 2011. The effect of alternative real-time wind forcing on Southern Ocean sea-ice simulations. *J. Geophys. Res.* 116, C11021.
- Swart, N.C., Fyfe, J.C., 2013. The influence of recent Antarctic ice sheet retreat on simulated sea ice area trends. *Geophys. Res. Lett.* 40, 4328–4332. <http://dx.doi.org/10.1002/grl.50820>.
- Talley, L.D., Pickard, G.L., Emery, W.J., Swift, J.H., 2011. *Descriptive Physical Oceanography: An Introduction*, sixth ed. Elsevier.
- Thompson, D.W.J., Solomon, S., 2002. Interpretation of recent southern hemisphere climate change. *Science* 296, 895–899.
- Toggweiler, J.R., Russell, J.L., Carson, S.R., 2006. Midlatitude westerlies, atmospheric CO<sub>2</sub>, and climate change during the ice ages. *Paleoceanography* 21, PA2005.
- Tournadre, J., Girard-Ardhuin, F., LeGrévy, B., 2012. Antarctic icebergs distributions, 2002–2010. *J. Geophys. Res.* 117, C05004. <http://dx.doi.org/10.1029/2011JC007441>.
- Turner, J., Bracegirdle, T.J., Phillips, T., Marshall, G.J., Hosking, J.S., 2013. An initial assessment of Antarctic sea ice extent in the CMIP5 models. *J. Clim.* 26, 1473–1484.
- Vancoppenolle, M., Fichefet, T., Goosse, H., 2009. Simulating the mass balance and salinity of Arctic and Antarctic sea ice. 2: Importance of sea ice salinity variations. *Ocean Model.* 27, 54–69.
- Vihma, T., Tuovinen, E., Savijärvi, H., 2011. Interaction of katabatic winds and near-surface temperatures in the Antarctic. *J. Geophys. Res.* 116. <http://dx.doi.org/10.1029/2010JD014917>.
- von Storch, J.S., Eden, C., Fast, I., Haak, H., Hernandez-Deckers, D., Maier-Reimer, E., Marotzke, J., Stammer, D., 2012. An estimate of Lorenz energy cycle for the world ocean based on the 1/10° STORM/NCEP simulation. *J. Phys. Oceanogr.* 42, 2185–2205.
- Washington, W.M., Parkinson, C.L., 2005. *An Introduction to Three-Dimensional Climate Modeling*. University Science Books, USA.
- Weber, M.E., Clark, P.U., Kuhn, G., Timmermann, A., Sprenk, D., Gladstone, R., Zhang, X., Lohmann, G., Menzel, L., Chikamoto, M.O., Friedrich, T., Ohlwein, C., 2014. Millennial-scale variability in Antarctic ice-sheet discharge during the last deglaciation. *Nature* 13397 (10.1038).
- Weijer, W., Sloyan, B.M., Maltrud, M.E., Jeffery, N., Hecht, M.W., Hartin, C.A., van Sebille, E., Wainer, I., Landrum, L., 2012. The Southern Ocean and its climate in CCSM4. *J. Clim.* 25, 2652–2675. <http://dx.doi.org/10.1175/JCLI-D-11-00302.1>.
- Whitworth III, T., Peterson, R.G., 1985. Volume transport of the Antarctic circumpolar current from bottom pressure measurements. *J. Phys. Oceanogr.* 15, 810–816.
- Worby, A.P., Geiger, C.A., Paget, M.J., Van Woert, M.L., Ackley, S.F., DeLiberty, T.L., 2008. Thickness distribution of Antarctic sea ice. *J. Geophys. Res.* 113, C05S92.
- Zhang, J., 2007. Increasing Antarctic sea ice under warming atmospheric and oceanic conditions. *J. Clim.* 20, 2515–2529.
- Zunz, V., Goosse, H., Massonnet, F., 2013. How does internal variability influence the ability of CMIP5 models to reproduce the recent trend in Southern Ocean sea ice extent? *Cryosphere* 7, 451–468.
- Zwally, H.J., Yi, D., Kwok, R., Zhao, Y., 2008. ICESat measurements of sea ice thickness in the Weddell Sea. *J. Geophys. Res.* 113, C02S15. <http://dx.doi.org/10.1029/2007JC004284>.